Norwegian Meteorological Institute
met.no
met.no report

no. 4/2004
Oceanography, Climate

Description of an integrated flux and sea-ice model suitable for coupling to an ocean and atmosphere model

Lars Petter Røed[1] **and Jens Debernard**
with contributions from
Øyvind Sætra, Morten Ødegaard Køltzow, and Jon Albretsen

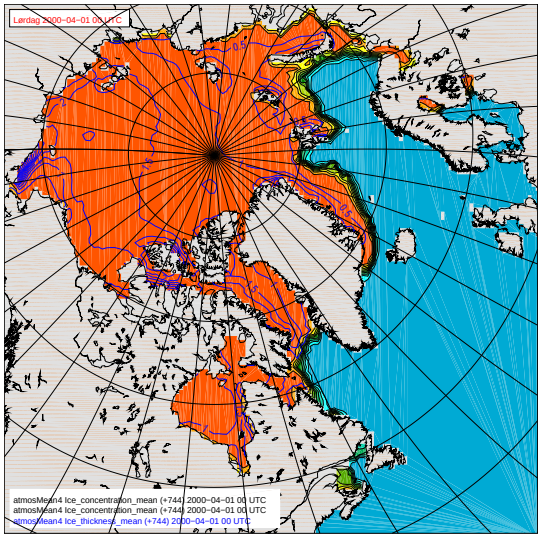

[1] Also affiliated with Department of Geophysics, University of Oslo, Norway

Norwegian Meteorological Institute
met.no

report

Title	**Date**
Description of an integrated flux and sea-ice model suitable for coupling to an ocean and atmosphere model	January 14, 2004
Section Oceanography	**Report no.** 4
Author(s)	**Classification**
Lars Petter Røed and Jens Debernard	● Free ○ Restricted
	ISSN 1503-8025
Client(s)	**Client's reference**
Research Council of Norway (RCN), EU 5th Framework Programme (EU)	155976/720, 143559/431, EVK2-2001-00337

Abstract

Considered is the most recent version of the dynamic-thermodynamic sea ice model MI-IM developed at the Norwegian Meteorological Institute. Its development is with a view to coupling to an atmosphere and an ocean model. In this the paramount principle is that fluxes exchanged between the ocean and the atmosphere are conserved. Since the heat flux parameterization in earlier versions of MI-IM did not conserve heat, the implementation of an additional thermodynamic variable, named the heat content or melt heat is introduced. The ice dynamics invokes the recently suggested elastic-viscous-plastic rheology which introduces the internal ice stress as a prognostic variable. The thermodynamics are similar to the Häkkinen-Mellor model, except for the introduction of the melt heat as a prognostic variable and some details regarding the computation of the incoming shortwave radiation and albedo. Special care has to be inferred when calculating the vertical fluxes exchanging heat and salinity between the atmosphere, cryosphere and hydrosphere. This necessitates to some degree that the type of atmosphere and/or ocean model to which the sea ice model is coupled is taken into account. The version of MI-IM documented below is coupled to the multilayer, isopycnic coordinate ocean model MICOM invoking MICOM's embedded upper mixed layer. The atmosphere model in mind is HIRHAM (High resolution limited area model - HIRLAM with ECMWF physics). However, the version documented and verified uses input from ECMWF's operational analysis. Presently all fluxes are calculated within the ice module, and hence no special coupler is invoked. Finally results from a thirty year verification run in which the coupled ice-ocean model was set up for the North Atlantic Ocean with a mesh size of about $1/2^o$ are shown. Acknowledging that this is a verification run the atmospheric forcing used is the two years 2000 and 2001 which was wrapped to produce a thirty year forcing. After about four to five years the model reach a quasi-equilibrium state in which the results almost repeat themselves in a two year cycle. The exception is the deep water circulation, which is to be expected. Due to the overflow of dense water from the Mediterranean Sea across the Strait of Gibraltar, and from the Nordic Seas across the Denmark Strait, the Faroe-Bank Channel, and the Wyville-Thomson Ridge, dense water is continuously spreading in the deeper parts of the North Atlantic.

Keywords Oceanography, climate, coupled models, air-sea fluxes

Disciplinary signature	**Responsible signature**

Postal address P.O Box 43 Blindern, N-0313 OSLO, Norway
Office Niels Henrik Abels vei 40
Telephone +47 2296 3000
Telefax +47 2296 3050
e-mail: met.inst@met.no
Internet: met.no
Bank account 7694 05 00601
Swift code DNBANOKK

Contents

List of Figures

List of Tables

1 Introduction

Below follows a documentation of the integrated flux and sea-ice model MI-IM which is the Norwegian Meteorological Institute's (met.no's) Ice Model). The present documented version is coupled to the Miami Isopycnic Coordinate Ocean Model (MICOM) (*Bleck et al.*, 1992), but with slight modification may be coupled to any ocean model whether it uses isopycnic, geopotential or σ-coordinates as its vertical coordinate. The development is part of the ongoing national climate project Regional Development under Global Climate Change (RegClim) and the EU Community 5th Framework Programme project Global implications of Arctic climate processes and feedbacks (GLIMPSE).

The overall task in RegClim is to produce estimates of the regional climate change suitable for impact assessments in Northern Europe, bordering sea areas and major parts of the Arctic (our region) given a global change. To achieve this goal one of the methods chosen is to dynamically downscale scenarios produced by atmosphere-ocean global circulation models (AOGCMs), which includes sea-ice as one of the relevant model components. As pointed out by *McAveney et al.* (2001) the quality of the global scenarios tends to deteriorate for subcontinental scales, which makes dynamical downscaling an attractive method in order to produce results amenable for assessment of societal and environmental impacts of climate change on a regional scale. Increased regional skill added to AOGCMs using stand alone atmosphere regional climate models (ARCMs), in which the sea state in terms of sea surface temperature (SST) and sea-ice cover is specified through the global scenario, are documented in, e.g., *Giorgi et al.* (2001) and *Denis et al.* (2002).

One of the characteristics of our region is its closeness to the Arctic, implying that a sea-ice cover exist throughout the whole year (present day climate). This implies that a detailed information on sea-ice extent, its concentration and its thickness is of significance for impact studies. Another characteristic is the vast area covered by an anomalously (with respect to latitude) warm ocean, a fact that is commonly believed to contribute significantly to the present day relatively warm climate of our region. In the dynamic downscaling performed through earlier phases in RegClim (*Bjørge et al.*, 2000; *Debernard et al.*, 2002; *Bjørge and Ødegaard*, 2000) an ARCM only is used. Hence a change in the atmospheric circulation is not accompanied by a change in sea-ice extent, ocean circulation or SST within the downscaled region. To ameliorate this situation it is chosen within the continuation of the RegClim project to develop a coupled atmosphere-ocean regional climate model (AORCM) for dynamical downscaling purposes. A documentation of the sea-ice model component and its integrated air-sea flux module (MI-IM) in the RegClim-AORCM is the focus of this report.

The dynamics in MI-IM are based on the elastic-viscous-plastic (EVP) rheology suggested by *Hunke and Dukowicz* (1997). Experiments with earlier versions of the sea-ice model, as for instance reported in *Sætra et al.* (1998) and *Røed et al.* (1999), show that the *Häkkinen and Mellor* (1992) model implemented early on in the project, tends to give too much ice and excessive ice thicknesses in areas featuring obstructions like islands and promontories. One possible explanation for this behavior is that the ice model is too stiff, and hence arrests the ice in areas where there are obstructions. This led naturally to consider the new ice dynamics based on the EVP rheology. It should be noted that the introduction of elasticity is a pure numerical

artifact and does not necessarily reflect any physical characteristics of the ice as a medium. One of the main advantages of the EVP rheology is that it allows the time step required by the numerical stability criterion for an explicit computation of the internal ice stresses to be dramatically increased, and thereby allows for the use of an explicit solution scheme rather than the slower and more cumbersome implicit elliptic solver commonly applied in pure viscous-plastic rheology models (*Hibler*, 1979). Thus the integration of the model equations becomes much more efficient on the computer, and hence more practical for use in long term climate simulations.

The thermodynamics expands on that suggested by *Mellor and Kantha* (1989) as formulated in *Häkkinen and Mellor* (1992). Regarding the incoming shortwave solar radiation its parameterization is more similar to that suggested by *Drange and Simonsen* (1996), while the parameterizations of the turbulent (latent and sensible) heat fluxes are more in line with the bulk formulas suggested by *Kara et al.* (2002). In addition an equation for the conservation of heat content in the ice is added. The heat content in this respect is defined as the thermal energy required to bring the ice volume to a reference temperature (here the melting temperature of sea ice). Moreover, a positive definite advection scheme known as MPDATA (*Smolarkiewicz*, 1983; *Smolarkiewicz and Margolin*, 1997), for the advection of ice thickness, ice concentration, and heat content is implemented. This minimizes the diffusion of the steep gradients in the dependent variables, and hence helps to retain a sharper ice edge in the marginal ice zone.

A vital part of the sea-ice model is its integrated air-sea flux module which conservatively exchange heat, salt and momentum between the three spheres atmosphere, cryosphere, and hydrosphere. This is achieved by computing fluxes to and from the various interfaces into the various spheres in a conservative fashion. There are four interfaces that must be considered: the atmosphere-snow interface (or atmosphere-ice when the ice is bare), the ice-snow interface, the ice-ocean interface, and the atmosphere-ocean interface. The fluxes computed are parameterized as bulk fluxes. For instance are the fluxes into the atmosphere from the atmosphere-snow (or atmosphere-ice) and atmosphere-ocean interfaces in the present version of MI-IM based on bulk formulas that involves knowledge of atmospheric variables such as the 2m temperature, the dew point temperature, the wind vector at 10 m height, mean sea level pressure, cloud fraction, etc., (*Kara et al.*, 2002).

For the exchange of properties across the interfaces to be conservative, the requirement is that the flux from one medium toward a specific interface and the flux into the other medium away from the same interface balances. This gives rise to the natural boundary condition that the interface value of the property in question is such that it satisfies this balance, a requirement used to compute the interface value of that property. To illustrate this consider the heat fluxes across the atmosphere-ocean interface. The oceanic heat flux toward the interface and the atmospheric heat flux away from the interface then both depends on the interface temperature and to balance them the interface temperature is adjusted accordingly. However, the interface temperature cannot drop below the freezing temperature (at that salinity). In that case the interface temperature is set equal to the appropriate freezing temperature which implies that the heat fluxes does not balance. Under these circumstances, and to ensure a conservative exchange of heat, ice is formed which stores the surplus energy. Similarly if the temperature at, e.g., the atmosphere-snow interface becomes larger than the melting temperature of snow, it must be set equal to the melting

temperature of snow in which case the imbalance of fluxes is used to compute the rate of snow melt. The ice-ocean interface is special in this regard since the temperature at that interface is always fixed at the freezing temperature of sea water. Hence the norm is that the oceanic heat flux toward the ice-ocean interface and the cryospheric heat flux away from the same interface do not balance, which implies that ice is continuously melted or produced there. Also worth mentioning is that it is desirable that a certain amount of summer melt water is stored on the ice-snow interface as melt ponds and refrozen in the fall due to its impact on the albedo. However, this is not yet implemented properly and is therefore not active in the present version of MI-IM.

Computing the interface temperatures based on a balance of heat fluxes across the various interfaces also have some additional advantages. For instance the calculation of air-sea heat fluxes in areas of open water is strongly dependent on the actual temperature used to represent the surface temperature at the atmosphere-ocean interface. This temperature impacts both the (upward) long wave radiation through the Stefan-Boltzmann law and the turbulent heat fluxes. Traditionally in ocean modeling, bulk formulas use either the temperature in the upper layer from a layer model, or the temperature at the uppermost level from a level model. However, in cases when an ocean model is forced with short-wave radiation which resolves the diurnal cycle, the amount of energy received by the ocean model may come out wrong simply because the interface temperature is too cool during the day and too warm during the night. To illustrate this, consider for example a situation with incoming solar radiation under cloud free condition. During the part of the day when the sun shines, the very thin uppermost skin of the ocean which is in direct contact with the atmosphere will warm rapidly due to radiative forcing. The oceanic bulk-temperature of the upper ocean on the other hand, is to a much stronger degree determined also by ocean dynamics, and hence, responds on a much longer time scale than does the interface temperature to incoming solar radiation. Due to this, the temperature difference between the uppermost few millimeters of the ocean surface and the underlying mixed layer may in some cases be of several degrees (*Fairall et al.*, 1996). During night time with strong cooling, the opposite takes place, resulting in a much colder atmosphere-ocean interface temperature relative to the oceanic mixed layer temperature. The conservative scheme chosen for MI-IM avoids this problem, and the model may also be run both with atmospheric data that resolves the diurnal cycle.

At met.no, MI-IM is also used as a forecasting tool. It is then coupled to met.no's operational ocean model MI-POM (*Engedahl*, 1995; *Engedahl et al.*, 2001; *Røed and Fossum*, 2003), a σ-coordinate or terrain-following coordinate ocean model, which is a version of the Princeton Ocean Model (*Blumberg and Mellor*, 1987). It should be emphasized that many of the models parameters and parameterizations are to some extent dependent on the actual ocean model used. In this respect, the process of coupling MI-IM to the two very different ocean models MI-POM and MICOM has been helpful when developing MI-IM.

The organization of this report is as follows. Section 2 offers some comments regarding the ice as a continuum, followed by an overview of the notation used (Section 3). Section 4 gives an account of the models prognostic variables, while Section 5 gives an overview of the models governing equations. Here the description of the governing equation for the heat content (Section 5.4) is more detailed than the others. Next follows Section 6 which describes the parameterization of the momentum fluxes. It is followed by Section 7 which describes the computation of the

various production rates (e.g., rate at which ice grows and/or melts, snow melts, precipitation, and others), and Section 8 describing in essence the boundary conditions and how the interface temperatures are computed. These sections establish the basis for the computation of the heat and salinity fluxes across the various interfaces as described in (Section 9) and (Section 10), respectively. Finally, results from a thirty year verification run is discussed in Section 11, while some final remarks are offered in Section 12. Also an Appendix is added which gives an overview of some of the Fortran programs (flowcharts).

2 Ice as a continuum

The governing equations for sea ice is given in a two-dimensional Cartesian coordinate system with the x- and y-axis in the horizontal plane. For the vertical fluxes, a z-axis which is positive upward (with respect to the direction of the gravitational acceleration) is applied.

It is furthermore assumed that the sea ice can be modeled as a continuum in which its presence is described by two-dimensional continuous variables in time and space. The variables are rendered continuous by defining the ice concentration (or the fraction of ice cover), A, as the fraction of a unit area ω actually covered by ice floes of individual areas ω_n and thicknesses h_n in the limit $\omega \to 0$, that is,

$$A \equiv \lim_{\omega \to 0} \sum_{n=1}^{N} \frac{\omega_n}{\omega}, \tag{1}$$

where N is the number of ice floes within the area ω. Accordingly the ice thickness, h is defined as the average thickness over that fraction, or

$$h \equiv \lim_{\sigma \to 0} \sum_{n=1}^{N} \frac{h_n \omega_n}{\omega}. \tag{2}$$

As pointed out by *Overland et al.* (1998) these definitions inherently assume that the resolution of the model is larger than the typical size of an ice floe. Assuming that the individual ice floes on average are smaller than one to two kilometers, it entails that the grid size of the model must be larger than say five to ten kilometers.

In the model a unit area is only totally covered by ice when the ice concentration attains its maximum value of 100%. Hence the usual state of affairs is that a unit area consists of both ice and open water as sketched in Figure 1, that is, $A < 1$. In addition to the pure ice layer the ice vertically also consists of a snow layer of thickness h_S.

Note that MI-IM, in contrast to more complex sea-ice models, is composed of two ice layers only. If more layers and/or categories are introduced (*Bitz and Lipscomb*, 1999), then each layer and/or category has a uniquely defined ice concentration and thickness in accord with (1) and (2).

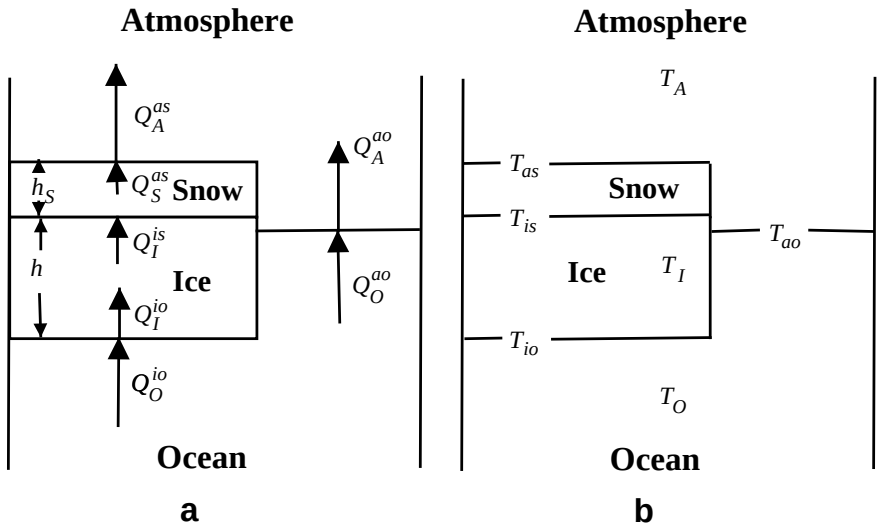

Fig. 1: Sketch of the vertical thermodynamic ocean-ice-snow-atmosphere model in MI-IM conveniently showing some of the notation used in the text. Panel a (left panel) shows the various heat fluxes, while panel b (right panel) shows the various temperatures used to calculate them. The temperatures and heat fluxes are listed in Tables 1 and 2, respectively. Note that the temperature at the ice-ocean interface $T_{io} \equiv T_f$, that is, is fixed at the salinity dependent freezing temperature of sea water as given in (3).

3 Notation, definitions and some basic assumptions

To separate between the four media atmosphere, ocean, snow, and ice the notation followed throughout is such that capital letters in a sub- or superscript is used to denote the medium (A = atmosphere, O = ocean, S = snow, and I = ice), while small letters is used to denote an interface. The model includes four interfaces (Figure 1), namely the ice-ocean interface (sub- or superscript io), the atmosphere-ocean interface (sub- or superscript ao), the ice-snow interface (sub- or superscript is), and the atmosphere-snow interface (sub- or superscript as)[2].

In Figure 1 is also displayed the key temperatures used to calculate the heat fluxes, which in turn is used to calculate the production rates. Here T_O is the temperature in the interior of MICOM's upper ocean mixed layer, T_I the temperature in the interior of the ice (thought of as an average over the ice thickness), and T_A the atmospheric temperature (at 2m height). The temperatures at the interfaces are T_{io}, the temperature at the ice-ocean interface T_{is}, the temperature at the ice-snow interface, T_{as} the temperature at the atmosphere-snow interface, T_{ao} the temperature at the atmosphere-ocean interface, and when the ice is bare T_{ai}, the temperature

[2]When the ice is bare (no snow) the two interfaces atmosphere-snow and ice-snow collapse into a single atmosphere-ice interface

Table 1: List of the various temperatures used to compute the heat fluxes. Note that temperatures at the various interfaces (except the temperature at the ice-ocean interface which equals the freezing temperature of sea water) are diagnostic variables computed in accord with the boundary condition at the interface in question. Numbers in parentheses refer to the equation number where the variable is first introduced. All temperatures are as a norm given in degree Celsius (^oC), but in certain parameterizations it is necessary to specify them in degree Kelvin (K).

Symbol	Description	Eq.
T_O	Upper ocean mixed layer temperature	(65)
T_{io}	Temperature at ice-ocean interface ($\equiv T_f$)	(60)
T_f	Freezing temperature of sea-water	(3)
T_{ao}	Temperature at atmosphere-ocean interface	(61)
T_{is}	Temperature at ice-snow interface	(56)
T_I	Interior ice temperature	(16)
T_{f0}	Melting temperature of freshwater ice	(55)
T_{as}	Temperature at the atmosphere-snow interface	(55)
T_{ai}	Temperature at atmosphere-ice interface	(59)
T_A	Atmosphere temperature at 2 m	(42)
T_A^s	Weighted interface temperature	(93)

at the atmosphere-ice interface. T_{ao} is also referred to as the skin sea surface temperature. The temperature T_{io} at the ice-ocean interface is special in that it is always fixed at the freezing temperature of sea water, hence $T_{io} \equiv T_f$, where T_f is the freezing temperature. It depends on the salinity and is given by

$$T_f = -\mu s_O \tag{3}$$

where μ is a constant (Table 5), and s_O is the salinity at the ice-ocean interface. Here it is assumed that s_O equals MICOM's upper mixed layer salinity. Note that μ is given in ^oC and hence that the unit for T_f in (3) is ^oC as well. Normally the freezing temperature deviates from the oceanic mixed layer temperature which gives rise to conductive heat fluxes between the ice and the ocean (Section 9.1.1). This is also true within the ice. Thus conductive heat fluxes also arise in the ice since the interior ice temperature, which is a true average over the ice thickness (Section 5.4), in general deviates from both the temperature at the ice-ocean interface and the ice-snow (or atmosphere-ice) interface.

Regarding the various heat fluxes displayed in Figure 1 the notation used is Q_X^{yy} where the subscript X refers to the medium in which the heat flux takes place, while the superscript yy refers to the interface which the heat flux is either directed toward or away from. All the heat fluxes computed in the model are listed in Table 2, and are directed *upward* when *positive*. Thus Q_O^{io} and Q_O^{ao} denote the oceanic heat flux toward the ice-ocean and atmosphere-ocean interface, respectively, Q_I^{io} the cryospheric heat flux away from the ice-ocean interface toward the interior of the ice, and so on. The snow layer is assumed to have no heat capacity implying that $Q_S^{as} = Q_I^{is}$.

The atmosphere-ice interface is special in the sense that it only exists as long as there there

Table 2: Net heat fluxes (unit W/m^2) computed in MI-IM and displayed in Figure 1. The column marked 'Intro' gives the equation number where the variable is first introduced, while the column 'Defined' gives the equation number where the variable is defined. The notation is such that a subscript denotes the medium (A = atmosphere, O = ocean, I = ice, S = snow) in which the heat flux takes place, while a superscript denote the interface (ao = atmosphere-ocean, ai = atmosphere-ice, as = atmosphere-snow, io = ice-ocean, is = ice-snow) toward which the heat flux is directed.

Symbol	Description	Intro	Defined
Q_O^{io}	In ocean toward the ice-ocean interface	(21)	(64)
Q_O^{ao}	In ocean toward the atmosphere-ocean interface	(21)	(64)
Q_I^{io}	In ice away from ice-ocean interface	(54)	(72)
Q_I^{is}	In ice toward the ice-snow interface	(55)	(73)
Q_S^{is}	In snow away from the ice-snow interface ($\equiv Q_I^{is}$)	(56)	(56)
Q_S^{as}	In snow toward the atmosphere-snow interface ($\equiv Q_S^{is}$)	(47)	(71)
Q_A^{as}	In atmosphere away from the atmosphere-snow interface	(21)	(82)
Q_A^{ao}	In atmosphere away from the atmosphere-ocean interface	(21)	(81)
Q_A^{ai}	In atmosphere away from the atmosphere-ice interface	(50)	(81)
Q_I^{ai}	In ice toward the atmosphere-ice interface	(50)	(73)

is no snow on the ice. Normally the snow cover vanishes sometimes during the spring. Under these circumstances the ice-snow and atmosphere-snow interfaces collapse into an atmosphere-ice interface. The heat flux notation for the cryospheric heat flux toward the atmosphere-ice interface is then changed to Q_I^{ai}, while the atmospheric heat flux away from the same interface is changed to Q_A^{ai}. The interface temperature is accordingly denoted T_{ai}.

It should be noted that as long a there is snow on the ice, the assumption that no heat can accumulate in the snow (the snow has no heat capacity) requires that

$$Q_S^{as} = Q_S^{is} = Q_I^{is}, \tag{4}$$

and hence that the heat flux toward the ice-snow interface from the ice interior always balances the heat flux in the snow away from the same interface. Because of this fact the two cases that the ice is snow covered or bare is sometimes treated separately below.

During bottom accretion (production of ice by freezing at the ice-ocean interface), or when ice is formed by freezing in open water, small pockets of brine becomes trapped in the ice. Hence the sea ice is saline. In the present version of MI-IM the ice salinity is assumed to be fixed such that it is zero at the top of the ice layer and two times its average value at the bottom of the ice layer. Thus the average ice salinity, s_I, is fixed (Table 5). The fact that the sea ice is saline affects both its specific heat, its conductivity, and thereby also its melting temperature, its heat content and the heat fluxes.

Finally, it is important to note that in most of the parameterizations used it is inherent that the temperatures are given in degrees Celsius (^oC), as for instance in (3). However, there are a few instances in which the temperature must be provided in degrees Kelvin (K), and if so it will be noted below.

Table 3: Prognostic variables in MI-IM. Number in parenthesis refers to the equation where the variable is first introduced

Symbol	Description	Eq.	Unit
A	Sea ice area (fraction from 0 to 1)	(5)	–
h	Sea ice thickness	(5)	m
$\mathbf{u}$	Sea ice velocity with components (u, v)	(5)	m/s
h_S	Thickness of snow layer	(6)	m
E	Heat content (or melt heat) of ice	(13)	J/m^2
$\mathcal{R}$	Stress tensor with components r_{ij} $(i, j = 1, 2)$	(27)	N/m

4 Prognostic variables

The main prognostic variables are the ice concentration A, the ice thickness h, and the ice velocity $\mathbf{u}$ with components u, v along the horizontal x- and y-axes (Table 3). In addition MI-IM also carries the thickness of the snow layer, h_S, the internal ice stress tensor $\mathcal{R}$, and the heat content E as prognostic variables.

The introduction of $\mathcal{R}$ as a prognostic variable is in accord with *Hunke and Dukowicz* (1997), who advocated the addition of a pure artifi cial time dependent elastic term in the ice rheology equation. This allows the governing equations to be solved (numerically) using an explicit method rather than the traditional and more cumbersome implicit method, and the model code to be more practical for parallelization. The introduction of the melt heat or heat content as a prognostic variable makes it possible for ice formed in one place to be melted in another location without violating heat conservation.

As is common the model also features a number of diagnostic variables related to its dynamics (e.g., ice pressure, shear and bulk viscosities) and thermodynamics (e.g., heat fluxes, interface temperatures, ice production, etc.). These are listed and described in their respective sections.

5 Governing equations

5.1 Conservation of ice mass

The ice mass m_I per unit area is simply the product of the ice thickness, the ice concentration and the ice density, that is, $m_I = \rho_I h A$ in which the ice density ρ_I is assumed to be constant (Table 4). The ice mass per unit area in one location changes in time due to advective fluxes and due to local sources and sinks (e.g., freezing and/or melting).

The present formulation for the time rate of change of m_I is based on that of *Mellor and Kantha* (1989) and includes advection, melting from above, melting and/or freezing from below, and lateral melting and/or freezing, that is,

$$\partial_t(hA) + \nabla \cdot (hA\mathbf{u}) = \frac{\rho_w}{\rho_I}\left[A(W_{io} - W_{ai}) + (1 - A)W_{ao}\right]. \tag{5}$$

Here ρ_w is the reference density of sea water (Table 4), W_{io} the ice production rate at the ice-ocean interface (*positive* under freezing), W_{ai} the production rate at the atmosphere-ice interface (*positive* under melting otherwise zero, hence the negative sign in front), and W_{ao} the production rate at the atmosphere-ocean interface (*positive* under freezing otherwise zero). All production rates are calculated in sea water equivalents, that is, in units of sea water height per unit time (hence the appearance of the factor ρ_w/ρ_I on the right-hand side). Note that W_{ai} is nonzero only when the ice is bare (no snow cover). If the ice is covered with snow the top surface becomes an ice-snow interface at which no ice production takes place. A detailed description of the production rates and their parameterizations is deferred to Section 7.

5.2 Conservation of snow mass

The snow mass m_S per unit area is similarly given as a product of the constant snow density ρ_S, the snow thickness h_S and the ice fraction A. The latter indicates that snow is only present in the ice covered portion of a unit area. Hence the snow mass per unit area is $m_S = \rho_S h_S A$.

The time rate of change of m_S depends on ice advection and local snow production (precipitation in the form of snow and snow melt) and ice advection. Hence its formulation is similar to (5) and reads,

$$\partial_t(h_S A) + \nabla \cdot (h_S A \mathbf{u}) = \frac{\rho_f}{\rho_S} A(W_s - W_{as}), \tag{6}$$

where ρ_f is the density of freshwater (Table 4), W_s is the snow production rate due to frozen precipitation minus evaporation, and W_{as} is the melting rate of snow. Both W_s and W_{as} are defi ned as positive defi nite quantities, and are calculated in freshwater equivalents, that is, given in units of freshwater height divided by time (hence the appearance of the factor ρ_f/ρ_S). Again the description of the actual expressions used to parameterize the production rates is deferred to Section 7.

Table 4: Physical constants used in the conservation equations for ice and snow masses per unit area, and ice fraction. Numbers in parentheses refer to the equation number where the constant is first introduced.

Symbol	Description	Eq.	Value	Unit
ρ_w	Reference density of sea water	(5)	1026	kg/m^3
ρ_I	Reference density of sea-ice	(5)	900	kg/m^3
ρ_f	Reference density of freshwater	(6)	1000	kg/m^3
ρ_S	Reference density of snow	(6)	300	kg/m^3
Φ_1	Empirical constant	(7)	0.7	–
Φ_2	Empirical constant	(7)	4.0	–

5.3 Conservation of ice concentration

Since only one equation can be derived from the principal of mass conservation of ice, an additional empirical equation must be outlined for the ice concentration. One obvious contribution to the time rate of change of the ice concentration is ice advection. Other sources are ice production (melting/freezing) in the ice covered portion of a unit area and the formation of ice in open water areas. Consider first the latter. As given in (5) the ice mass (or ice column) formed is given by $(1 - A)W_{ao}$. The question then arises how to distribute this increase between the ice thickness and ice concentration? Secondly when ice is melting and/or freezing in that portion of a unit area that is already covered by ice (given by $A(W_{io} - W_{ai})$), what is the reciprocal change in the ice concentration?

These questions are resolved in MI-IM by introducing empirical constants as suggested by *Mellor and Kantha* (1989). Hence the time rate of change of ice concentration is

$$\partial_t A + \nabla \cdot A\mathbf{u} = \frac{\rho_w}{h\rho_I}\left[-\Phi_1 A(W_{ai} - W_{io})H(W_{ai} - W_{io}) + \Phi_2(1 - A)W_{ao}\right]. \tag{7}$$

Here $H(\xi)$, equal to 1 for $\xi > 0$ and 0 for $\xi \leq 0$, is Heaviside's unit function, and Φ_1 and Φ_2 are the two empirical constants (Table 4). The use of Heaviside's unit function implies that as long as $W_{io} \geq W_{ai}$, implying that the ice volume increases (more ice is formed by freezing from below than melted from above) no change in ice concentration is experienced (remembering that W_{ai} is a positive definite quantity), that is, all the ice volume produced is converted into an increase in the ice thickness. On the other hand when $W_{io} < W_{ai}$, implying that the melting from above is more efficient than the freezing of ice from below (or that ice is melting both from above and below), the ice concentration decreases with a factor determined by the empirical constant Φ_1. Note that when this occurs, and to avoid changing the snow thickness, the surplus snow volume is dumped in the upper ocean mixed layer, which gives rise to what is later referred to as snow run off (Section 7.3). Since W_{ao} is a positive definite quantity, the last term on the right-hand side of (7) implies that when ice freezes in the open water patches the ice concentration increases with a factor determined by the second empirical constant Φ_2.

How the empirical constants Φ_1 and Φ_2 regulates how the ice volume production is distributed on thickness and concentration is perhaps more clearly exhibited if (5) and (7) are combined to give an equation for the ice thickness only, that is,

$$\begin{aligned} A\left(\partial_t h + \mathbf{u} \cdot \nabla h\right) = \frac{\rho_w}{\rho_I}\big\{ & A(W_{io} - W_{ai})\left[1 - \Phi_1 H(W_{ai} - W_{io})\right] \\ & + (1 - \Phi_2)(1 - A)W_{ao}\big\}. \end{aligned} \tag{8}$$

Thus if $\Phi_2 = 1$ none of the ice formed at the atmosphere-ocean interface changes the ice thickness, only the ice concentration changes. Likewise if $\Phi_1 = 1$ then all the net ice melt in the ice covered portion of a unit area is exploited to decrease the ice fraction, that is, lateral melt.

5.4 Conservation of heat content

Besides the fact that the sea ice changes the surface albedo, isolates the atmosphere from the ocean, and alters the atmosphere-ocean momentum exchange, it also acts as a heat reservoir. In

Table 5: Physical constants used to establish the conservation equation for heat content. Number in parenthesis indicates equation number where the constant is first introduced

Symbol	Description	Eq.	Value	Unit
μ	Physical constant used in (3), (9)	(3)	0.0543	$^oC/psu$
c_{pf}	Specifi c heat of freshwater ice	(10)	2093	J/kgK
L_w	Latent heat of fusion	(10)	$3.347 \cdot 10^5$	J/kg
s_I	Average salinity of sea ice	(14)	3.2	psu

fact, in open ocean areas where the atmosphere is cold the atmospheric heat flux away from the atmosphere-ocean interface may become larger than the oceanic heat flux toward the same interface if the interface temperature drops below the freezing temperature of sea water. In that case the heat defi cit is stored as sea-ice. Subsequently the ice is advected to another location where it melts. Thus to obtain a conservative heat exchange at the atmosphere-ocean interface also the internal thermodynamics of the sea-ice model must conserve heat. Moreover, when coupling atmosphere, ice and ocean models, which is the object here, it is of paramount importance that the total heat transferred between the various spheres are conserved, including the ice medium. This was a problem in earlier versions of met.no's ice model, e.g., *Sætra et al.* (1998) and *Sætra et al.* (1999). In the version of MI-IM documented here this problem is solved by introducing a new prognostic variable, named the heat content (or melt heat), which simply measures the thermal energy required to melt all ice in a vertical column.

While details regarding the development of (5) - (8) is found in *Mellor and Kantha* (1989) and *Häkkinen and Mellor* (1992), a more detailed discussion is justifi ed for the development of a prognostic equation that conserves the heat content. This new equation replaces the governing equation for the interior ice temperature used in the earlier versions of MI-IM, as for instance reported in *Sætra et al.* (1998) and *Sætra et al.* (1999), and also that reported in *Häkkinen and Mellor* (1992). Since the ice salinity is fi xed the evolution of the interior ice temperature T_I is embedded in the new prognostic equation describing the evolution of the heat content.

5.4.1 Thermal energy

The development starts with noting the fact that sea ice differs from freshwater ice. Each time sea ice is formed at the atmosphere-ocean and/or the ice-ocean interface a small amount of salt becomes trapped in the ice in the form of small pockets containing a salt solution, commonly referred to as brine pockets. The small, but most striking consequence is a lowering of the melting temperature of the ice compared to freshwater ice. Given that the salinity of a parcel of sea ice, s_{ice}, is between 1 and 8 psu, its melting temperature T_m (in ^oC) is approximated by

$$T_m = -\mu s_{ice}, \tag{9}$$

or the same expression as used to calculate the freezing temperature of sea water, that is, (3), where μ is an empirical constant as given in Table 5. The most important difference however

appears for ice colder than the melting point. Since sea ice consists of both pure ice (that is, freshwater ice) and brine pockets, the specifi c heat capacity of a parcel of sea ice is

$$c_{ice} = c_{pf} - L_w \frac{T_m}{T_{ice}^2}, \tag{10}$$

where T_{ice} is the temperature of an ice parcel (measured in ^oC), L_w is the latent heat of fusion, and c_{pf} is the (constant) specifi c heat of freshwater ice (Table 5). The rationale behind (10) is that for a parcel of sea ice that consists of a mix of freshwater ice and brine pockets to experience a temperature rise of ΔT the freshwater part requires an amount of thermal energy (per unit mass) of $c_{pf}\Delta T$, while the brine pockets requires an additional amount of thermal energy (per unit mass) given by

$$-L_w \int_{T_{ice}}^{T_{ice}+\Delta T} \frac{T_m}{T'^2_{ice}} dT'_{ice} = L_w \left(\frac{T_m}{T_{ice}} - \frac{T_m}{T_{ice}+\Delta T} \right). \tag{11}$$

Thus the total thermal energy (per unit mass) needed to raise the temperature of a parcel of saline sea-ice from a given initial temperature T_{ice} to its melting temperature T_m is then

$$q = \int_{T_{ice}}^{T_m} c_{ice}(T'_{ice}) dT'_{ice} = c_{pf}(T_m - T_{ice}) + L_w \left(1 - \frac{T_m}{T_{ice}} \right). \tag{12}$$

To illuminate the difference between the behavior of freshwater ice and sea-ice (12) is illustrated in Figure 2. For fresh ice (dashed line), the energy required to increase the temperature to its melting temperature is small. However, when the temperature reaches the melting point, a large amount of energy is required simply because the energy needed to change freshwater ice to water is much larger than the energy needed to change its temperature. For sea ice, the picture is somewhat different (solid line). Noting that $(T_m/T_{ice}^2) \leq 0$ it follows from (10) that its heat capacity (or specifi c heat) is always larger than that of freshwater ice. Thus when the sea ice temperature increases a large amount of energy actually goes into melting the ice surrounding the brine pockets, that is, to increase the brine volume. As the temperature gets closer to the melting temperature a considerable amount of sea ice is already melted. Therefore, as illustrated in Figure 2, the energy required to melt sea ice close to its melting point is considerably smaller and always less than the comparable energy required to melt warm freshwater ice.

This particular property of sea ice has some important consequences for the design of sea-ice models. One of the simplest designs treats the ice as pure freshwater ice while neglecting its heat capacity. Then heat storage is in the form of latent heat only, which as revealed by Figure 2 contains most of the effect of the ice as a heat reservoir. It is possible to construct a heat-conserving sea ice model with this approach. However, according to *Bitz and Lipscomb* (1999), this results in an overestimation of the seasonal variations in ice-thickness. In addition the ice tends to melt too early in spring/summer and to freeze too early in the fall. In MI-IM it is therefore opted to include a salinity dependent heat capacity in accord with (10). In this the average ice salinity and its profi le through the ice is kept constant as indicated in (14) and (15).

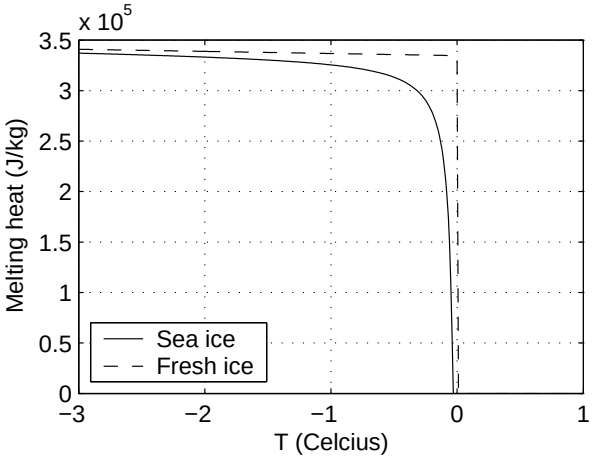

Fig. 2: The thermal energy per unit mass (or melting heat) needed to raise the temperature of sea ice (solid curve) and freshwater ice (dashed curve) to its respective melting temperatures as computed from (12).

5.4.2 Heat content

To conserve heat content the energy stored in the ice must then be advected in the same manner as the other ice variables. Thus an additional thermodynamic variable E, dubbed the heat content (or melt heat), is introduced. In accord with (12), and the fact that the ice in MI-IM only consist of one layer, it is simply defi ned as the energy required to raise all the parcels of sea ice within a vertical ice column to its melting temperature. Thus,

$$E = \rho_I A \int_0^h q dz, \tag{13}$$

where q is given by (12), and h is the ice thickness. Note that q is a function of z through its dependence of $T_{ice}(z)$ and $T_m(z)$.

To simplify (13) further the salinity profi le is assumed to be linear with zero salinity at the ice-snow interface and such that it attains its average value,

$$s_I = \frac{1}{h} \int_0^h s_{ice} dz, \tag{14}$$

in the middle of the ice layer. It then follows that

$$s_{ice}(z) = -\frac{2s_I}{h}(z - h) \tag{15}$$

implying that the salinity at the ice bottom is $2s_I$. Furthermore defi ning the average temperature and average melting temperature in the ice layer by

$$T_I = \frac{1}{h} \int_0^h T_{ice} dz, \quad T_{mI} = \frac{1}{h} \int_0^h T_m dz = -\mu s_I, \tag{16}$$

respectively, and substituting q from (12) into (13), E becomes

$$E = \rho_I A h \left[c_{pf} \left(T_{mI} - T_I \right) + L_w \left(1 - \frac{1}{h} \int_0^h \frac{T_m}{T_{ice}} dz \right) \right]. \tag{17}$$

To resolve the integral on the right-hand side of (17) knowledge about the temperature profile within the ice is required. In contrast to the salinity the temperature may attain any profile within the ice. It is constrained however to equal the freezing temperature of sea water (3) at the bottom of the ice layer, and to equal the temperature at the ice-snow interface (or atmosphere-ice interface if the ice is bare) at the top of the ice layer. Considerable temperature shears may therefore develop adjacent to the respective interfaces and a linear temperature profile is hardly adequate. Let the temperature be written $T_{ice} = T_I + T'$ where T' is the temperature deviation. Then, assuming that the temperature profile in the ice do not deviate too much from the average temperature T_I, that is, assuming that $T'/T_I << 1$, E is to lowest order approximated by

$$E = \rho_I A h \left[c_{pf} \left(T_{mI} - T_I \right) + L_w \left(1 - \frac{T_{mI}}{T_I} \right) \right], \tag{18}$$

which is the expression used for E in MI-IM. Note that (18) also follows directly from (13) if the temperatures T_m and T_{ice} are approximated by their averages T_{mI} and T_I, respectively, in (10) and (12).

Expression (18) may also be used to define the latent heat of fusion L_I of saline sea ice, that is,

$$L_I \equiv \frac{E}{\rho_I A h}, \tag{19}$$

which by use of (18) reads,

$$L_I = L_I(s_I, T_I) = c_{pf}(T_{mI} - T_I) + L_w(1 - \frac{T_{mI}}{T_I}). \tag{20}$$

5.4.3 Conservation equation

In accord with the other prognostic variables a conservation law for E is now formulated as

$$\partial_t E + \nabla \cdot (\mathbf{u} E) = A \Delta Q_{ice} + (1 - A) \Delta Q_{ao}. \tag{21}$$

where $\Delta Q_{ao} = Q_A^{ao} - Q_O^{ao}$ is the gain in heat due to a difference in the heat flux at the atmosphere-ice interface (open water) and ΔQ_{ice} is the total heat gain in the already ice covered area, that is,

$$\Delta Q_{ice} = \left\{ \begin{array}{ll} Q_S^{is} - Q_O^{io} & ; h_S > 0 \\ Q_A^{ai} - Q_O^{io} & ; h_S = 0 \end{array} \right\} = \Delta Q_I + \Delta Q_{io} - \Delta Q_{ai}, \tag{22}$$

where in turn $\Delta Q_{io} = Q_I^{io} - Q_O^{io}$ is the heat gain due to production of ice at the ice-ocean interface, $\Delta Q_{ai} = Q_I^{ai} - Q_A^{ai}$ is the heat gain due to production of ice at the atmosphere-ice interface, and

$$\Delta Q_I = \left\{ \begin{array}{ll} Q_I^{is} - Q_I^{io} & ; h_S > 0 \\ Q_I^{ai} - Q_I^{io} & ; h_S = 0 \end{array} \right. . \tag{23}$$

is the heat gain due to a difference in the heat fluxes into the ice.

As alluded to above an equation for the time rate of change of the interior ice temperature T_I is embedded in (21). Noting that $T_{mI} = -\mu s_I$ is constant, it follows from (18) that E is a function of ice concentration, ice thickness, and T_I only. Let in accord with (10)

$$c_I = c_{pf} - L_w \frac{T_{mI}}{T_I^2} \tag{24}$$

be the average specific heat of sea ice. Then by combining (21) and (5), and making use of (18), an equation for T_I follows, viz.,

$$\partial_t T_I + \mathbf{u} \cdot \nabla T_I = \frac{1}{\rho_I h A c_I} \left\{ A \left(W_{io} - W_{ai} - \frac{\Delta Q_{ice}}{\rho_I L_w} \right) + (1 - A) \left(W_{ao} - \frac{\Delta Q_{ao}}{\rho_I L_w} \right) \right\}, \tag{25}$$

which may be compared to the one of *Häkkinen and Mellor* (1992, p. 20,288). As is obvious the ice production terms depends on the flux differences across the various interfaces. Indeed, using the expressions developed in Section 7 for W_{io}, W_{ai}, and W_{ao}, (25) becomes

$$\partial_t T_I + \mathbf{u} \cdot \nabla T_I = \frac{\Delta Q_I}{\rho_I h c_I}, \tag{26}$$

where ΔQ_I is as given by (23), that is, the temperature change in the ice is proportional to the difference in the cryospheric heat fluxes at the top and the bottom of the ice layer.

The introduction of E as the new prognostic variable provides the means by which the internal heat content in sea-ice is conserved. For instance, examine the horizontal integral of (21) over a finite closed domain assuming that no advection takes place through the lateral boundaries. Then the total change in E is exactly matched by any imbalance in the heat fluxes between the atmosphere and the ocean.

5.5 Conservation of momentum

As is common the nonlinear terms for Eulerian advection of momentum are assumed to be small and are hence neglected. The momentum equation thus reads

$$m_I \partial_t \mathbf{u} = \nabla \cdot \mathcal{R} - m_I f \mathbf{k} \times \mathbf{u} + A \boldsymbol{\tau}_{ai} + A \boldsymbol{\tau}_{io} - m_I g \nabla H_o \tag{27}$$

Here,

$$\mathcal{R} = r_{ij} \mathbf{i}_i \mathbf{i}_j \quad i, j = 1, 2 \tag{28}$$

is a two dimensional stress tensor describing the internal stresses in the ice. The Coriolis parameter is given by $f = 2\Omega \sin \phi$, where Ω is the angular frequency of the earth (Table 7) and ϕ is the latitude. Furthermore, g is the gravitational acceleration (Table 7) and H_o is the sea surface elevation (provided by MICOM). The stresses (or momentum fluxes) acting at the ice-ocean and atmosphere-ice interfaces are respectively given by $\boldsymbol{\tau}_{io}$ and $\boldsymbol{\tau}_{ai}$ as detailed in Section 6.

Table 6: Diagnostic variables in the conservation equation (27) for momentum. Numbers in parenthesis refer to the equation number where the variable is first introduced.

Symbol	Description	Eq.	Unit
m_I	Ice mass per unit area (=$\rho_I h A$)	(27)	kg/m^2
P	Sea ice pressure	(29)	N/m
ζ	Shear viscosity	(29)	kg/s
η	Bulk viscosity	(29)	kg/s
$\dot{\mathcal{E}}$	Strain rate tensor with components $\dot{\varepsilon}_{ij}$ $(i,j=1,2)$	(29)	$1/s$

5.5.1 Internal ice stress

As alluded to, the stress tensor (28) is computed prognostically using the elastic-visco-plastic rheology and method suggested by *Hunke and Dukowicz* (1997). This is in contrast to the traditional method introduced by *Hibler* (1979) who applied a pure visco-plastic rheology in which the internal ice stress is computed diagnostically in combination with (27). In that case the internal stress is given by (*Hibler*, 1979)

$$\mathcal{R} = 2\eta\dot{\mathcal{E}} + \left[(\zeta-\eta)\dot{\mathcal{E}} : \mathcal{I} - \frac{P}{2}\right]\mathcal{I} \tag{29}$$

where P is the internal ice pressure, η and ζ are nonlinear shear and bulk viscosities, $\dot{\mathcal{E}}$ is the (symmetric) strain rate tensor given by

$$\dot{\mathcal{E}} = \frac{1}{2}\left(\nabla\mathbf{u} + \nabla\mathbf{u}^T\right) = \dot{\varepsilon}_{ij}\mathbf{ij} \tag{30}$$

and $\mathcal{I}$ is the unit tensor[3].

To solve (27) numerically using an explicit solver with the stress given by (29) requires the use of time steps less than one second for a mesh size of about 100 km. The application of such a small time step severely slows down the speed by which the calculations for a given simulation period can be performed, in particular if the model is going to be used for long term climate simulations. For this reason the traditional approach has been to abandon the explicit solver and to employ implicit solvers. The introduction of an implicit solver is however cumbersome when the code is to be prepared for parallel machines.

Following *Hunke and Dukowicz* (1997) this is avoided by introducing a time dependent (elastic) term in the rheology equation. To this end (29) is first rewritten to give

$$\frac{1}{2\eta}\mathcal{R} + \frac{1}{4\zeta}\left[\frac{(\eta-\zeta)}{\eta}\mathcal{R} : \mathcal{I} + P\right]\mathcal{I} = \dot{\mathcal{E}}. \tag{31}$$

[3]The notation $\mathcal{A} : \mathcal{B}$ entails that the vector product should be performed twice. Thus $\mathcal{A} : \mathcal{B} = a_{ij}b_{ji}$, where a_{ij} and b_{ij} are the components of $\mathcal{A}$ and $\mathcal{B}$, is a scalar.

Table 7: Physical constants used in the conservation equation (27) for momentum and in the calculation of the internal ice stress. Numbers in parenthesis indicate equation number where the constant is first introduced.

Symbol	Description	Eq.	Value	Unit
g	Gravitational acceleration	(27)	9.806	m/s^2
Ω	Earth's rotation rate	(27)	$0.7292 \cdot 10^{-4}$	$1/s$
c	Exponential factor ice pressure	(34)	20	$-$
P^*	Ice strength	(34)	10^4	N/m
e	Eccentricity of the yield curve	(35)	2.0	$-$
E_0	Elasticity constant appearing in	(37)	0.25	$-$

Then the time dependent term is introduced by rewriting (31), viz.,

$$\frac{1}{E_m}\partial_t \mathcal{R} + \frac{1}{2\eta}\mathcal{R} + \frac{1}{4\zeta}\left[\frac{(\eta-\zeta)}{\eta}\mathcal{R} : \mathcal{I} + P\right]\mathcal{I} = \dot{\mathcal{E}}. \tag{32}$$

where E_m is an elasticity modulus. An explicit numerical solution of the momentum equation, taking into account (32), now involves a time step restriction, which in the one dimensional case amounts to

$$\Delta t \leq \sqrt{\frac{m_I}{E_m}}\Delta x, \tag{33}$$

to be numerically stable (Δx is the grid size and Δt is the time step). Thus the time step criterion for a numerical solution becomes dependent on the elasticity modulus and is affected in such a way that an explicit solution is practical. It is important to note that the elastic term introduced in (32) is not meant to represent any real physics, but is simply a convenient work around the problem imposed by the short time step limitation for the explicit numerical solution. It is therefore important later to try to minimize the effect of this term on the ice physics.

It remains to defi ne the ice pressure P and the bulk and shear viscosities ζ, η that appears in (32). Following *Hibler* (1979) and *Hunke and Dukowicz* (1997) these are diagnostic variables in which P is calculated as a function of the ice thickness and concentration, viz.,

$$P = P^* A h e^{-c(1-A)}, \tag{34}$$

where c and P^* are constants (Table 7), while ζ and η are calculated from the ice pressure as

$$\zeta = \frac{P}{2\Delta} \leq 2.5 \cdot 10^8 P, \quad \eta = \frac{\zeta}{e^2}. \tag{35}$$

Here

$$\Delta = \left[(1+e^{-2})\dot{\varepsilon}_{ij}^2\delta_{ij} + 4e^{-2}\dot{\varepsilon}_{12}^2 + 2(1-e^{-2})\dot{\varepsilon}_{11}\dot{\varepsilon}_{22}\right]^{1/2}, \tag{36}$$

where e is the eccentricity of the yield curve (Table 7) and $\dot{\varepsilon}_{ij}$ are the components of the strain rate tensor (30). Note that a maximum value is set on the bulk viscosity ζ. Hence (35) implies that there is also an upper bound on the shear viscosity η.

Table 8: Physical constants used to compute the stresses on the atmosphere-snow, atmosphere-ice, ice- ocean and atmosphere-ocean interfaces. Numbers in parenthesis indicate equation number where the constant is first introduced.

Symbol	Description	Eq.	Value	Unit
ρ_A	Reference atmospheric density	(38)	1.267	kg/m^3
C_D^{ai}	Drag coeffi cient at the atmosphere-ice interface	(38)	$1.5 \cdot 10^{-3}$	–
C_D^{io}	Drag coeffi cient at the ice-ocean interface	(39)	$3.8 \cdot 10^{-3}$	–
λ	Turning angle of ice-ocean stress	(39)	23	$degrees$
γ_A	Gas constant of dry air	(41)	287.0	m^2/Ks^2
W_A^{max}	Maximum atmospheric wind speed used to compute the drag coeffi cient C_{Df}^{ao}	(45)	32.5	m/s
W_A^{min}	Minimum atmospheric wind speed used to compute the drag coeffi cient C_{Df}^{ao}	(45)	2.5	m/s

What remains is simply to choose the elasticity modulus E_m so that an explicit solution is practical, and at the same time making sure that the effect of introducing elasticity is minimized. In the present version it is given by the formula

$$E_m = 2m_I E_0 \left[\min\left(\frac{\Delta x}{\Delta t}, \frac{\Delta y}{\Delta t} \right) \right]^2 \tag{37}$$

where E_0 is a constant less than one (Table 7). This choice ensures that the CFL criterion (33) is satisfi ed.

6 Momentum fluxes

The wind stress that appears in (27) is related to the 10 meter wind speed $\mathbf{U}_A$ (with components U_A, V_A along the x- and y-axis, respectively) through the relation

$$\boldsymbol{\tau}_{ai} = \rho_A C_D^{ai} |\mathbf{U}_A| \mathbf{U}_A \tag{38}$$

where ρ_A is a reference air density (Table 8) and C_D^{ai} is a non-dimensional drag coeffi cient for the momentum transfer between the atmosphere and the ice (Table 8). Normally the atmospheric wind speed is much larger than the ice speed, which explains the negligence of the ice velocity in (38).

In similarity with the atmosphere-ice stress, as given by (38), the stress acting on the ice-ocean interface depends on the upper layer ocean current $\mathbf{U}_O$. However, since $\mathbf{U}_O$ and the ice velocity $\mathbf{u}$ has the same order of magnitude, the difference between them has to be taken into account. Thus,

$$\boldsymbol{\tau}_{io} = \rho_w C_D^{io} |\mathbf{U}_O - \mathbf{u}| \left[(\mathbf{U}_O - \mathbf{u}) \cos\lambda + \mathbf{k} \times (\mathbf{U}_O - \mathbf{u}) \sin\lambda \right], \tag{39}$$

where C_D^{io} is a non-dimensional drag coefficient (Table 8) and λ is a turning angle (Table 8). In the present implementation $\mathbf{U}_O$ is the depth independent (bulk) velocity of the upper (mixed) layer in MICOM.

The final momentum flux is that over open water, that is, the stress $\boldsymbol{\tau}_{ao}$ acting on the atmosphere-ocean interface. Besides providing the kinetic energy input into the open ocean, this flux is also needed to determine the ice growth in open water (Section 9.1, eq. 69). Presently the parameterization used to compute $\boldsymbol{\tau}_{ao}$ is the one suggested by *Kara et al.* (2000) and *Kara et al.* (2002), that is,

$$\boldsymbol{\tau}_{ao} = \rho_{Af} C_{Df}^{ao} |\mathbf{U}_A| \mathbf{U}_A. \tag{40}$$

where ρ_{Af} is the surface air density and C_{Df}^{ao} is a non-dimensional drag coefficient at the atmosphere-ocean interface. In turn ρ_{Af} is given by the ideal gas formula (*Gill*, 1982, p. 41), that is,

$$\rho_{Af} = \frac{p_A}{\gamma_A T_A}, \tag{41}$$

where p_A is the mean sea level pressure (in Pa), T_A is the 2m air temperature (in ^{o}K), and γ_A is the gas constant of dry air (Table 8). The drag coefficient C_{Df}^{ao} depends on the 10m atmospheric wind speed $|\mathbf{U}_A|$, and the difference between T_A and the atmosphere-ocean interface temperature T_{ao} through the formula

$$C_{Df}^{ao} = C_{D0}(W_A) + C_{D1}(W_A)(T_{ao} - T_A), \tag{42}$$

where the coefficients C_{D0} and C_{D1} are

$$C_{D0} = 10^{-3}\left(0.692 + 0.071 W_A - 0.0007 W_A^2\right), \tag{43}$$

and

$$C_{D1} = 10^{-3}\left(0.083 - 0.0054 W_A - 0.000093 W_A^2\right), \tag{44}$$

respectively, where

$$W_A = \max\left[W_A^{min}, \min\left(|\mathbf{U}_A|, W_A^{max}\right)\right]. \tag{45}$$

7 Production rates

Processes that leads to a change in the heat content and or salinity of the atmosphere, ice or ocean may all be parameterized as production rates[4] given in units of length per time. The processes considered in MI-IM are: (i) freezing and melting of ice at the ice-ocean interface which leads to a production rate denoted W_{io}, (ii) freezing of ice at the atmosphere-ocean interface which leads to a production rate W_{ao}, (iii) lateral melting of snow due to an equal lateral change in the ice fraction. This snow melt is referred to as run off and a parameterized as a production rate W_{ro}, (iv) vertical melting of ice at the ice-snow interface which leads to a production rate W_{ai}, (v) melting of snow at the atmosphere-snow interface which leads to a production rate W_{as}, and

Table 9: List of ice and snow production rates at the various interfaces. All rates are given in freshwater equivalents and in m/s. The column 'Intro' refers to the equation number where the variable is first introduced, while the column 'Defined' refers to the equation number where the variable is defined.

Symbol	Description	Intro	Defined
W_{io}	Production at the ice-ocean interface	(5)	(54)
W_{ai}	Production at the atmosphere-ice interface	(5)	(50)
W_{ao}	Production at the atmosphere-ocean interface	(5)	(53)
W_s	Frozen precipitation (snow)	(6)	(48)
W_{as}	Vertical melt rate of snow	(6)	(47)
W_r	Wet precipitation (rain)	(49)	(49)
W_{ro}	Snow run off due to lateral melting of snow covered ice	(51)	(51)

(vi) precipitation either in the form of wet precipitation (rain) at a rate W_r or frozen precipitation (snow) at a rate W_s. In the latter two also the evaporation is included.

All production rates at the various interfaces connected to melting and freezing of ice and/or snow are calculated in water equivalents and according to the generic formula

$$W_{xx} = \frac{\Delta Q}{\rho L} \tag{46}$$

where ΔQ is the flux imbalance at the interface in question, ρ is an appropriate density, and L is a pertinent heat of fusion. The subscript xx is used to refer to the interface in question. The remaining production rates are either specified (as is precipitation) or are more subtle (as, e.g., snow run off). Table 9 provides a list of the various production rates.

Note that any melted ice is immediately given to the upper ocean mixed layer (here MICOM) as a fresh and/or brackish water source and thus gives rise to both a heat flux (Section 9) and a salinity flux (Section 10). Hence no melt water nor rain is stored at the atmosphere-ice or ice-snow interface in the present version of MI-IM. In the same vein it should also be mentioned that ice production due to formation of frazil ice (ice production in the upper ocean mixed layer) is not yet properly implemented in MI-IM, although some exploratory experiments with frazil ice formation are already performed with success at the time of writing.

7.1 Atmosphere-snow interface

As long as there is snow on the ice an atmosphere-snow interface exists. Here snow can be produced either by atmospheric deposition of snow (frozen precipitation) or by melting.

Melting of snow can only occur if the interface temperature T_{as} at the atmosphere-snow interface equals the melting temperature of snow, i.e., $T_{as} = 0^oC$. When this occurs there is

[4]Production rates as used here may be negative or positive, e.g., the production rate due to ice formed by freezing is a positive quantity whereas the production rate due to melting of ice is a negative quantity.

an imbalance in the fluxes across the interface (see Section 8.1) so that $Q_A^{as} < Q_S^{as}$. Thus the production rate of snow due to vertical melting of snow is given by

$$W_{as} = \frac{Q_S^{as} - Q_A^{as}}{\rho_f L_w} H(Q_S^{as} - Q_A^{as}), \tag{47}$$

where $H(\xi)$ is Heaviside's unit function[5]. Note that the sign convention is such that W_{as} is positive under melting as required. As alluded to in the introduction to this Section the melt water produced when $W_{as} > 0$ is transferred directly to the ocean as a freshwater source, and hence impacts both the heat and salinity fluxes. Melt ponds that later may refreeze are not allowed in the present version of MI-IM.

When snow is falling it accumulates at a rate given by the precipitation P_{snow}. At the same time snow evaporates by sublimation to the atmosphere at a rate E_{subl}. The production rate due the combination of precipitation and sublimation, denoted W_s, is thus

$$W_s = \frac{\rho_S}{\rho_f}(P_{snow} - E_{subl}), \tag{48}$$

where the factor ρ_S/ρ_f appears to ensure that W_s is given in freshwater equivalents. It should also be noted that W_s is given for the entire unit cell and is hence in (6) multiplied by the ice fraction A (see also Section 7.4). Finally, while the precipitation is a direct input from the atmosphere model, the sublimation is calculated in MI-IM.

Precipitation may also be in the form of wet precipitation (rain) denoted P_{rain}, and in the spring it may even fall before the snow has melted. In reality some of the rain water is absorbed by the snow and used to alter the snow density. This is, however, not an option in the present version of MI-IM. Here the rain water is transferred directly to the ocean at a rate

$$W_r = (P_{rain} - E_{evap}), \tag{49}$$

where E_{evap} is the evaporation. Again the precipitation is inferred directly from the atmospheric input while the evaporation is calculated in MI-IM.

7.2 Ice-snow interface

As long as there is snow on the ice the ice-snow interface temperature $T_{is} < 0^oC$. Hence there is now production of ice at this interface before the atmosphere-snow and ice-snow interface collapse into the atmosphere-ice interface. The computation of T_{is} is detailed in Section 8.2.

7.3 Atmosphere-ice interface

Because of the assumption that the snow has no heat capacity ice is only allowed to melt at its top surface when the ice is bare, that is, when its top surface becomes an atmosphere-ice

[5] W_{as} is denoted wsm in MI-IM's FORTRAN code. Note also that W_{as} is calculated in freshwater equivalents, hence the use of the freshwater density and L_w.

interface. Moreover, even if the ice is bare it only starts to melt when $T_{ai} = 0^oC$, that is, when the atmosphere-ice interface temperature equals the melting temperature of sea-ice.[6] In accord with the boundary condition at the atmosphere-ice interface (Section 8.3) this condition can only prevail if $Q_I^{ai} > Q_A^{ai}$, that is, as long as the cryospheric heat flux toward the atmosphere-ice interface is larger than the atmospheric heat flux away from the same interface. Hence the production rate W_{ai} at the atmosphere-ice interface is

$$W_{ai} = \frac{Q_I^{ai} - Q_A^{ai}}{\rho_w L_I} H(Q_I^{ai} - Q_A^{ai}). \tag{50}$$

When $W_{ai} > 0$ the melt water thus created, as with melted snow, is transferred directly to the ocean as a freshwater source impacting both the heat and salinity fluxes. In the spring when the transition from snow covered to bare ice occurs, the heat flux imbalance during one time step may be larger than the amount necessary to melt the remaining snow. In that case the surplus energy is used to melt ice in accord with (50).

Finally, it is noted from (7) that a nonzero W_{ai} leads to a decrease in the ice fraction, that is, lateral melting of ice. In accord with the conservation equation for snow mass (6) this also changes the fraction of a unit area covered by snow by an equal amount. To keep the remaining snow thickness constant under this process the surplus snow is simply dumped into the ocean. This is called snow run off and the associated rate W_{ro} at which snow is transferred to the ocean (as freshwater) is given by

$$W_{ro} = -\frac{h_S}{\Delta t}\frac{\rho_S}{\rho_f}\Delta A^*, \tag{51}$$

where

$$\Delta A^* = \Phi_1 A \frac{\Delta t}{h}\frac{\rho_w}{\rho_I}(W_{io} - W_{ai})H(W_{ai} - W_{io}) \tag{52}$$

is the change in the ice fraction due to lateral melting of ice in the time step Δt as detailed in (7).

7.4 Atmosphere-ocean interface

As long as the atmosphere-ocean interface temperature (T_{ao}) is larger than the freezing temperature of sea water (T_f) as given by (3) no ice forms at the atmosphere-ocean interface (Section 8.5). However, when $T_{ao} = T_f$ the oceanic heat flux toward the atmosphere-ocean interface (Q_O^{ao}) is not balanced by the atmospheric heat flux away from the same interface (Q_A^{ao}). To conserve heat, ice then starts to form at a rate given by the imbalances in the two fluxes, that is,

$$W_{ao} = \frac{Q_A^{ao} - Q_O^{ao}}{\rho_w L_I} H(Q_A^{ao} - Q_O^{ao}), \tag{53}$$

where the sign convention that W_{ao} should be positive under freezing is followed.

During the summer season Q_A^{ao} in the Arctic is dominated by the incoming solar radiation (as is Q_A^{ai} and/or Q_A^{as}, and hence Q_A^{ao} is mostly negative during this period. As a consequence it then

[6] As noted in Section 5.4.2 the ice at the ice-ocean interface is completely fresh (no salinity) so that the melting temperature of sea-ice at the top equals the freezing temperature of freshwater, that is, equals 0^oC

inhibits the formation of ice in open water or leads ($W_{ao} = 0$). At the end of the summer season the incoming shortwave radiation, however, rapidly becomes smaller and hence T_{ao} starts to drop and quickly becomes equal to the freezing temperature of sea water ($W_{ao} > 0$), at which time ice starts to form in open water areas in accord with (53). Finally, it should be noted that also the precipitation minus evaporation rates as given by (48) and (49) must be considered, whether it is wet precipitation (rain) or frozen precipitation (snow).

7.5 Ice-ocean interface

This interface is special in the sense that the boundary condition demands that $T_{io} \equiv T_f$ (Section 8.4). Hence the oceanic heat flux Q_O^{io} toward this interface is usually not balanced by the cryospheric heat flux Q_I^{io} away from the same interface. Hence the production rate W_{io} at this interface is given by

$$W_{io} = \frac{Q_I^{io} - Q_O^{io}}{\rho_w L_I}, \tag{54}$$

where the sign convention that W_{io} is positive under freezing and negative under melting is followed.

8 Boundary conditions and temperatures at the model's interfaces

As alluded to in Section 2 the temperatures at the various interfaces (Table 1 and Figure 1) are computed so as to satisfy the boundary conditions at the various interfaces. The latter requires that as long as the temperature at the interface in question differs from its freezing or melting point, then the heat fluxes to and from the interface must equal. This condition is utilized to compute the interface temperatures until they reach their freezing or melting temperature. If on the other hand the fluxes do not balance the difference is used to produce ice as detailed in Section 7, while the boundary condition is replaced by the condition that the interface temperature in question equals its respective melting or freezing temperature.

8.1 Atmosphere-snow interface

When the ice is snow covered and $T_{as} < 0^oC$, that is, the temperature at the atmosphere-snow interface is less than the melting temperature of snow (the snow is assumed to be frozen freshwater), the boundary condition reads

$$Q_A^{as} = Q_S^{as} \quad ; T_{as} < 0^oC. \tag{55}$$

Since the heat fluxes (Section 9) are functions of the interface temperature, (55) is used to compute T_{as}. If on the other hand $T_{as} = 0^oC$, then the fluxes are recomputed using $T_{as} = 0^oC$ and, to conserve energy, the heat flux imbalance in turn used to melt snow. In that case W_{as} as defined in (47) becomes non-zero and by use of (6) the snow thickness changes. Note that the melted

snow is transferred (without delay) into the ocean as a freshwater source. Hence it gives rise not only to a heat flux, but also a salinity flux. The former is detailed in Section 9, while the latter is detailed in Section 10.

8.2 Ice-snow interface

As alluded to several times above, the snow has no heat capacity. Hence, (4) is valid, that is,

$$Q_I^{is} = Q_S^{is}. \tag{56}$$

This implies that $T_{is} < 0^o C$, or that the interface temperature at the ice-snow interface, T_{is}, is always less than its melting temperature. Hence ice can only melt from above when the ice becomes bare (no snow).

To compute the interface temperature it is noted that (Section 9.2)

$$Q_I^{is} = \frac{2k_I}{h}\left(T_I - T_{is}\right), \quad \text{and} \quad Q_S^{is} = \frac{k_S}{h_S}\left(T_{is} - T_{as}\right), \tag{57}$$

which by use of (56) gives

$$T_{is} = \frac{k_{is}T_I + T_{as}}{1 + k_{is}} \quad ; k_{is} = \frac{2k_I h_S}{k_S h}. \tag{58}$$

Note that when the ice becomes bare ($h_S \to 0$) then $T_{is} \to T_{as} = T_{ai}$. Thus no discontinuity is experienced in the interface temperature at the ice-snow interface when the ice-snow and atmosphere-snow interfaces collapse into the atmosphere-ice interface.

8.3 Atmosphere-ice interface

Next consider that the ice is bare. Then the boundary condition demands (look at Figure 1)

$$Q_A^{ai} = Q_I^{ai} \quad ; \quad T_{ai} < 0^o C. \tag{59}$$

Note that the melting temperature at the top of the ice is set to $0^o C$ since it is assumed that here the salinity is zero. If the equality of the fluxes in (59) gives $T_{ai} = 0^o C$ then T_{ai} is set equal to $0^o C$ and the fluxes in (59) is recomputed. The resulting flux imbalance is then used to melt ice at a rate W_{is} as detailed in Section 7.

8.4 Ice-ocean interface

The ice-ocean interface is special. Here the interface temperature is identical to the freezing temperature (3) of sea water at all times, or

$$T_{io} = T_f \tag{60}$$

Thus as a norm $Q_O^{io} \neq Q_I^{io}$, that is, the fluxes do not balance. As above the imbalance is used to calculate the production rate term W_{io} in (5) as detailed in Section 7.

8.5 Atmosphere-ocean interface

Finally the temperature T_{ao} at the atmosphere-ocean interface is determined by the boundary condition

$$Q_O^{ao} = Q_A^{ao} \quad ; \quad T_{ao} > T_f \tag{61}$$

As above the equality in (61) is first used to compute the interface temperature T_{ao}. If this results in $T_{ao} = T_f$, then T_{ao} is set equal to T_f and the fluxes in (61) is recomputed. Commonly under these circumstances $Q_O^{ao} \neq Q_A^{ao}$, and the difference is used to compute the ice production rate W_{ao} at the atmosphere-ocean interface as detailed in Section 7.

9 Heat fluxes

As outlined in the preceding section the production rates that appears in (5), (6), (7), (8), and (21) are all determined by imbalances in the heat fluxes at the various interfaces. These heat fluxes are listed in Table 2 and displayed in Figure 1. Following the sign conventions in Section 3 the heat fluxes are directed upward when positive and downward when negative. Also note that each of them are computed by adding several contributions, some directed upward and some downward. The heat fluxes listed in Table 2 are therefore the *net heat fluxes* toward or away from the interface in question. The sub- and superscript notation used is explained in Section 3. Besides the interface temperatures the heat fluxes also make use of a few other temperatures as listed in Table 1.

9.1 Oceanic heat fluxes

The heat flux from the ocean toward the ocean surface naturally decomposes into two parts (Figure 1). The first, Q_O^{io}, is the heat flux from the upper ocean mixed layer toward that portion of a unit area covered with ice[7], i.e., toward the ice-ocean interface (see Table 2), while the second, Q_O^{ao}, is the heat flux toward that portion of a unit cell which is open water, that is, toward the atmosphere-ocean interface. The net heat flux per unit area from the ocean toward the ocean surface is then the weighted sum of the two contributions, that is,

$$Q_O = AQ_O^{io} + (1 - A)Q_O^{ao} + Q_{ro}, \tag{62}$$

where Q_{ro} is the heat flux due to the snow run-off (Section 7.3) transferred to the ocean at the rate given in (51). Thus

$$Q_{ro} = \rho_f L_w W_{ro} \tag{63}$$

The heat fluxes Q_O^{io} and Q_O^{ao} has in turn two contributions, that is,

$$Q_O^{io} = Q_O^{io,cond} + Q_O^{io,sw} \text{and } Q_O^{ao} = Q_O^{ao,cond} + Q_O^{ao,sw}. \tag{64}$$

where $Q_O^{io,cond}$ and $Q_O^{ao,cond}$ are due to the (turbulent) heat conduction and $Q_O^{io,sw}$ and $Q_O^{ao,sw}$ stem from the incoming shortwave radiation. Note that the solar radiation is able to penetrate both the

[7] In the Fortran code this flux is referred to as FT (or ft)

snow and the ice layer and hence to provide a heat flux contribution to the upper ocean mixed layer not only in the open water areas but also in the ice covered areas.

9.1.1 Ice-ocean interface

The turbulent heat flux due to conduction toward the ice-ocean interface is parameterized as suggested by *Omstedt and Wettlaufer* (1992). Hence,

$$Q_O^{io,cond} = \rho_w c_{pw} C_{ht}^{io} |\Delta \mathbf{U}| (T_O - T_f), \tag{65}$$

where ρ_w is the density of sea water (Table 4), T_O is the upper ocean mixed layer temperature, c_{pw} is the specific heat of sea water (Table 10), and C_{ht}^{io} is the heat transfer coefficient (Table 10). $|\Delta \mathbf{U}| = |\mathbf{U}_O - \mathbf{u}|$ is the absolute value of the velocity difference between the ice and ocean, $\mathbf{U}_O$ being the upper ocean mixed layer velocity.

The penetrating shortwave radiation in the ice covered portion is parameterized by

$$Q_O^{io,sw} = -I_0 \exp(-\gamma_p h) \tag{66}$$

where

$$I_0 = \gamma_i (1 - \alpha_i) Q_{sw} \begin{cases} (h_S^{max} - h_S)/h_S^{max} & ; h_S < h_S^{max} \\ 0 & ; h_S \geq h_S^{max} \end{cases}, \tag{67}$$

is the shortwave radiation that penetrates the ice-snow interface, h is the ice thickness, γ_i (Table 10) is a constant ($0 < \gamma_i < 1$) determining the fraction of the net incoming shortwave radiation that penetrates the ice-snow interface, α_i is the albedo at the atmosphere-ice/snow interface (Section 9.3.1, eq. 84), h_S is the snow thickness, h_S^{max} (Table 10) is the maximum snow thickness that allows penetration of the shortwave radiation through the snow, and Q_{sw} is the incoming shortwave solar radiation (Section 9.3.2). Since Q_{sw} and I_0 both are positive the minus sign appearing in (66) ensures that $Q_O^{is,sw}$ is a downward directed flux in line with the sign convention of Section 3.

9.1.2 Atmosphere-ocean interface

The contribution to the oceanic heat flux toward the atmosphere-ocean interface due to heat conduction is given by

$$Q_O^{ao,cond} = \rho_w c_{pw} C_{ht}^{ao} u_* (T_O - T_{ao}), \tag{68}$$

where C_{ht}^{ao} is the heat transfer coefficients (Table 10) and u_* is the friction velocity parameterized by

$$u_* = \max\left(\sqrt{|\boldsymbol{\tau}_{ao}|/\rho_w}, u_*^{min}\right). \tag{69}$$

Here u_*^{min} is a minimum value (Table 10) and $\boldsymbol{\tau}_{ao}$ (Section 6) is the wind stress acting at the atmosphere-ocean interface (open water areas). The use of a minimum value u_*^{min} for the friction velocity reflects the fact that there is always a background turbulence even when the wind stress is very weak or negligible.

Table 10: Physical constants used in the calculation of oceanic and cryospheric heat fluxes. Number in parenthesis refers to equation number where the constant is first introduced.

Symb.	Description	Eq.	Value	Unit
c_{pw}	Specific heat of sea water	(64)	3990	J/kgK
C_{ht}^{io}	Transfer coefficient under ice	(65)	$2.0 \cdot 10^{-4}$	$-$
C_{ht}^{ao}	Transfer coefficient open water	(68)	0.02	$-$
u_*^{min}	Minimum friction velocity	(68)	0.001	m/s
γ_p	Constant determining the damping of shortwave radiation through the ice	(66)	1.4	m^{-1}
h_S^{max}	Maximum snow thickness allowing penetration of shortwave radiation	(67)	0.1	m
γ_i	Constant determining the fraction of shortwave radiation penetrating the ice-snow interface	(67)	0.8	$-$
γ_o	Constant determining the fraction of shortwave radiation penetrating the atmosphere-ocean interface	(70)	0.8	$-$
k_w	Conductivity of freshwater ice	(76)	2.04	W/mK
k_S	Conductivity of snow	(76)	0.256	W/mK

The fraction of the incoming solar radiation (shortwave radiation) that is allowed to penetrate into the ocean from the atmosphere-ocean interface is in accord with (66) and (67) parameterized by

$$Q_O^{ao,sw} = -\gamma_o(1-\alpha_o)Q_{sw}, \tag{70}$$

where γ_o (Table 10) is a constant ($0 < \gamma_o < 1$) determining the fraction of the incoming shortwave radiation that penetrates through the atmosphere-ocean interface to heat the upper ocean mixed layer, and α_o is the albedo at the atmosphere-ocean interface (Section 9.3.1).

9.2 Cryospheric heat fluxes

The cryospheric heat fluxes (Table 2) contains the heat fluxes in the ice as well as the snow. The first, Q_I^{io} is from the ice-ocean interface toward the ice interior, the second, Q_I^{is}, is from the ice interior toward the ice-snow interface, the third, Q_S^{is}, is from the ice-snow interface toward the snow interior and the fourth and last, Q_S^{as}, is the heat flux toward the atmosphere-snow interface from the snow interior. When the ice is bare the ice-snow and atmosphere-snow interfaces collapse into the atmosphere-ice interface, in which case and Q_I^{is} is replaced by Q_I^{ai}.

Since the snow has no heat capacity the two heat fluxes in the snow, in accord with (4), are equal. Moreover, they are assumed to be true conductive heat fluxes. Thus

$$Q_S^{as} = Q_S^{is} = \frac{k_S}{h_S}(T_{is} - T_{as}). \tag{71}$$

In similarity to the oceanic heat fluxes also the heat fluxes in the ice consist of two parts, one associated with heat conduction and a second associated with the downward penetrating shortwave radiation. Thus,

$$Q_I^{io} = Q_I^{io,cond} + Q_I^{io,sw}, \tag{72}$$

and

$$Q_I^{is} = Q_I^{is,cond} + Q_I^{is,sw} \; ; h_S > 0 \tag{73}$$

$$Q_I^{ai} = Q_I^{ai,cond} + Q_I^{ai,sw} \; ; h_S = 0 \tag{74}$$

9.2.1 Ice-ocean interface

Assuming that the average ice temperature T_I is a measure of the temperature in the middle of the ice, then the contribution to Q_I^{io} due to heat conduction is

$$Q_I^{io,cond} = \frac{2k_I}{h}(T_f - T_I), \tag{75}$$

where T_f is the freezing temperature of sea water, and k_I is the thermal ice conductivity. In accord with (*Häkkinen and Mellor*, 1992) the latter depends on the brine fraction r through the formula

$$k_I = k_w \max(1 - 1.2r, 0.25). \tag{76}$$

Here k_w (Table 10) is the conductivity of freshwater ice, and the brine fraction is defined by

$$r = \frac{T_{mI}}{T_I} = \frac{-\mu s_I}{T_I}. \tag{77}$$

Note that T_{mI} and T_I in (77) are to be given in ^oC. In MI-IM it is required that $s_I \neq 0$ psu and hence that $T_{mI} < 0^oC$. Thus, since $T_{mI} \leq T_I \leq 0^oC$, it follows that $0 < r \leq 1$. The minimum value of the thermal conductivity introduced in (76) reflects the fact that a brine solution has about 1/4 of the conductivity of fresh ice.

Regarding the contribution from the shortwave radiation it is noted that no net accumulation of heat due to this radiation is allowed at the ice-ocean interface, and hence by use of (66) that

$$Q_I^{io,sw} = Q_O^{io,sw} = -I_0 \exp(-\gamma_p h). \tag{78}$$

9.2.2 Ice-snow interface

In accord with (75) the contribution to the cryospheric heat flux toward the ice-snow interface due to heat conduction is parameterized by

$$Q_I^{is,cond} = \frac{2k_I}{h}(T_I - T_{is}). \tag{79}$$

The contribution due to the shortwave radiation is the fraction of the net incoming shortwave radiation at the ice-snow interface that penetrates the ice-snow interface. Thus,

$$Q_I^{is,sw} = -I_0, \tag{80}$$

where I_0 is as given in (67).

9.2.3 Atmosphere-ice interface

When the ice is bare (no snow) the ice-snow interface becomes an atmosphere-ice interface. Under these circumstances Q_I^{is} is replaced by Q_I^{ai} as given in (74). The conductive part $Q_I^{ai,cond}$ is found by replacing T_{is} in (79) by T_{ai}, while the shortwave contribution given in (80) is unaltered, except that the albedo changes in accord with (84) ($h_S = 0$).

9.3 Atmospheric heat fluxes

Also the heat flux toward the atmosphere from the topmost layer of a unit area (Figure 1) decomposes into two parts. The first, Q_A^{ao}, is the net heat flux from the atmosphere-ocean interface (open water) toward the atmosphere. The second is the net atmospheric heat flux away from the respective interface in the ice covered areas. This flux is denoted Q_A^{as} if the ice is snow covered ($h_S > 0$) or Q_A^{ai} if the ice is bare ($h_S = 0$). The parameterizations of these fluxes are quite similar and are, as is common, mostly composed of radiative and turbulent (latent and sensible) heat fluxes. Thus,

$$Q_A^{ao} = -(1 - \alpha_O)Q_{sw} - \varepsilon_O Q_{lw} + Q_{Se}^{ao} + Q_{La}^{ao} + Q_{pe} + \varepsilon_O \sigma T_{ao}^4, \tag{81}$$

and

$$Q_A^{as,ai} = -(1 - \alpha_I)Q_{sw} - \varepsilon_I Q_{lw} + Q_{Se}^{as,ai} + Q_{La}^{as,ai} + \varepsilon_I \sigma T_{as,ai}^4, \tag{82}$$

respectively. Here α_I is the albedo at the atmosphere-snow/ice interface, α_O is the albedo at the atmosphere-ocean interface as detailed in Section 9.3.1 below, and ε_I and ε_O are the respective emissivities (Table 11). Note that the sub- and superscript as in (82) is to be used when the ice is snow covered ($h_S > 0$), while the sub- and superscript ai is to be used if the ice is bare ($h_S = 0$). With this in mind the last term on the right-hand side of (81) and (82) is the outgoing long-wave radiation from respectively the atmosphere-ocean and the atmosphere-snow/ice interfaces, where σ is Stefan-Boltzmann constant (Table 11). The heat fluxes appearing in (81) and (82) are as follows. Q_{sw} is the incoming (downward) shortwave (solar) radiation and Q_{lw} is the similar incoming (downward) long-wave radiative flux. $Q_{Se}^{as,ai}$ is the turbulent sensible heat flux at the atmosphere-ice/snow interface and $Q_{La}^{as,ai}$ is the similar latent heat flux, while Q_{Se}^{ao} and Q_{La}^{ao} are the sensible and latent heat fluxes at the atmosphere-ocean interface. Finally, Q_{pe} appearing in (81) represents the heat flux due to melting of solid precipitation (snow) falling in open water areas, that is,

$$Q_{pe} = \rho_S L_w P_{snow}. \tag{83}$$

9.3.1 Surface albedo

The surface albedo depends on several factors (*Perovich and Grenfell*, 1981; *Grenfell et al.*, 1994; *Curry et al.*, 1996; *Tschudi et al.*, 2001). When snow is present on the ice the albedo generally increases. In turn the albedo of snow depends on the grain size, which again depends on snow age, temperature and whether the snow is wet or dry. For bare ice ($h_S = 0$), the albedo may depend on type of ice (young ice, multi year ice), ice thickness, and brine volume and

Table 11: Physical constants used in the atmospheric heat flux parameterizations. Number in parentheses indicate the equation number where the constant is first introduced.

Symbol	Description	Eq.	Value	Unit
h_{min}	A minimum ice thickness	(84)	0.5	m
θ_d^{max}	Maximum declination	(89)	23.44	$degrees$
σ	Stefan-Boltzmann's constant	(81)	$5.67 \cdot 10^{-8}$	J/m^2K^4s
ε_O	Emissivity if sea water	(81)	0.97	–
ε_S	Emissivity if snow	(81)	0.97	–
ε_I	Emissivity if sea ice	(82)	0.97	–
S_0	Solar constant	(90)	1367.0	W/m^2
L_V	Latent heat of evaporation	(96)	$2.501 \cdot 10^6$	J/kg
L_S	Latent heat of sublimation	(100)	$2.834 \cdot 10^6$	J/kg
C_{La}^{as}	Transfer coeffi cient latent heat (ice covered areas)	(100)	$1.5 \cdot 10^{-3}$	–
c_{pa}	Specifi c heat of atmosphere	(107)	1004	J/kgK
C_S^a	Transfer coeffi cient sensible heat (ice covered areas)	(107)	$1.2 \cdot 10^{-3}$	–

melting/non-melting conditions. In addition, formation of melt ponds during summer leads to a decrease in the albedo. The albedo of melt ponds in turn depends on depth, sediments in the water and the underlying ice. Typical values for the albedo are 0.7-0.9 for snow, 0.5-0.7 for directly exposed sea-ice and 0.2-0.4 for melt ponds. In addition to surface characteristics the albedo also depends on the zenith angle and the amount of cloud cover, a dependence of importance in the Arctic.

In MI-IM the albedo at the atmosphere-ice/snow interfaces is denoted α_i and is parameterized as a function of ice and snow thicknesses and atmospheric temperature according to the formula

$$\alpha_I = \begin{cases} 0.1 + (0.63 - 0.1)\min(h, h_{min})/h_{min} & ; \quad h_S = 0 \\ 0.75 & ; \quad h_S > 0, T_{as} = 0^oC \\ 0.80 & ; \quad h_S > 0, T_{as} < 0^oC \end{cases}, \tag{84}$$

where h_{min} is a minimum ice thickness below which the albedo starts to decrease (Table 11). This reflects the fact that when the ice becomes thin enough its inherent transparency makes it look darker and hence it absorbs more heat below a critical minimum thickness. When the ice thickness becomes very small the albedo tends toward the albedo of open water. Instead of using the number generated by the parameterization of this albedo as given by (85) below, the approximate number 0.1 is used.

In open water (atmosphere-ocean interface) the albedo is parameterized according to *Ebert and Curry* (1993), that is,

$$\begin{aligned} \alpha_O = {} & 0.518\left[(\alpha^* + 0.008)(1 - C_{lf}) + 0.06C_{lf}\right] \\ & + 0.482\left[(\alpha^* - 0.007)(1 - C_{lf}) + 0.06C_{lf}\right]. \end{aligned} \tag{85}$$

Here C_{lf} is the cloud fraction (specified as part of the atmospheric input), while α^* is the Earth's albedo outside the atmosphere. The latter depends on the solar altitude angle θ_z through the formula

$$\alpha^* = \frac{0.026}{\mu_0^{1.7} + 0.065} + 0.015(\mu_0 - 0.1)(\mu_0 - 0.5)(\mu_0 - 1) \tag{86}$$

where

$$\mu_0 = \max(\cos\theta_z, 0) \tag{87}$$

and the solar altitude at every hour in the day is derived from

$$\cos\theta_z = \sin\phi\sin\theta_d + \cos\phi\cos\theta_d\cos\left[\frac{\pi}{12}(12 - d_h)\right] \tag{88}$$

where in turn ϕ is the latitude, d_h is the local time of the day (in hours), and θ_d is the declination of the Earth's axis with respect to the suns equatorial plane, or

$$\theta_d = \theta_d^{max}\frac{\pi}{180}\cos\left[\frac{\pi}{d_y}(d_y - 2d_d)\right], \tag{89}$$

where d_y is the number of days in the year, d_d the day number of the year, and θ_d^{max} is the maximum of θ_d (Table 11).

9.3.2 Downward shortwave radiation, Q_{sw}

The downward shortwave radiation Q_{sw} depends on the time of the day, the solar altitude, and the cloud cover through the formula

$$Q_{sw} = \frac{S_0\mu_0}{2R_{an}^2}\left[0.7^{\mu_0^{-1}} + (1 - 0.9)\right](1 - 0.62C_{lf} - 0.0019\theta_z^0). \tag{90}$$

Here S_0 is the solar constant (Table 11),

$$R_{an} = 1 + 0.0167\sin\left[\frac{2\pi(d_d - 186)}{d_y}\right] \tag{91}$$

is the normalized Earth-sun distance, and

$$\theta_z^0 = \theta_z|_{d_h=12}. \tag{92}$$

is the zenith angle.

9.3.3 Downward longwave radiation, Q_{lw}

The (downward) long-wave radiation Q_{lw} is computed by using a slightly changed version of the formula suggested by *Rosati and Miyakoda* (1988) based on Stefan-Boltzmann law, that is,

$$Q_{lw} = \gamma_{lw}\sigma T_A^{s\,4} - 4\sigma T_A^{s\,3}(T_A^s - T_A). \tag{93}$$

Here γ_{lw} is

$$\gamma_{lw} = 1 - \left(0.39 - 0.005\sqrt{\varepsilon_s^A}\right)\left[1 - (0.5 + |\phi|\frac{0.4}{90.0})C_{lf}^2\right], \tag{94}$$

where in turn ϕ is the latitude and ε_s^A is the saturated vapor pressure in the atmosphere at 2m height (Section 9.3.4, eq. 104). T_A^s is a weighted (atmosphere) interface temperature given by

$$T_A^s = \left[AT_{as,ai}^4 + (1-A)T_{ao}^4\right]^{1/4} \tag{95}$$

where the surface temperatures at the atmosphere-ocean interface, T_{ao}, and the atmosphere-snow (or atmosphere-ice) interface, $T_{as,ai}$, must be provided in K.

9.3.4 Latent heat fluxes, Q_{La}^{ao}, $Q_{La}^{as,ai}$

The parameterization of the latent heat fluxes differ slightly whether the ocean surface is ice covered or not. In the open water areas the latent heat flux is parameterized in accord with *Kara et al.* (2002). Hence

$$Q_{La}^{ao} = \rho_{Af} L_V C_{Lf}^{ao} |\mathbf{U}_A| (q_{ao} - q_A), \tag{96}$$

where ρ_{Af} is the surface air density as given in (41), L_V is the latent heat of evaporation (Table 11), C_{Lf}^{as} is the transfer coefficients of latent heat over open water as detailed below in (97), $\mathbf{U}_A$ is the atmospheric wind at 10 m, q_{ao} is the specific humidity at the atmosphere-ocean interface, and q_A is the atmospheric specific humidity. The transfer coefficient is

$$C_{Lf}^{ao} = C_{L0}(W_A) + C_{L1}(W_A)(T_{ao} - T_A), \tag{97}$$

where the coefficients C_{L0} and C_{L1} are given by

$$C_{L0} = 10^{-3}\left(0.8195 + 0.0506W_A - 0.0009W_A^2\right), \tag{98}$$

and

$$C_{L1} = 10^{-3}\left(-0.0154 - 0.5698\frac{1}{W_A} - 0.6743\frac{1}{W_A^2}\right), \tag{99}$$

respectively. In the above three formulas W_A denotes the air speed as defined in (45).

The latent heat flux in ice covered areas is simpler and given by

$$Q_{La}^{as,ai} = \rho_A L_S C_{La}^{as} |\mathbf{U}_A| (q_{as,ai} - q_A), \tag{100}$$

where ρ_A is the reference air density (Table 11), L_S is the latent heat of ice sublimation (Table 11), C_{La}^{as} is the transfer coefficient of latent heat over ice/snow (Table 11), and $q_{as,ai}$ is the specific humidity at the atmosphere-snow (or atmosphere-ice) interface.

The specific humidities that enters (96) and (100) are computed according to the formula given in *Rogers and Yau* (1989), viz.,

$$q = 0.622\frac{\varepsilon_s}{p_A - 0.378\varepsilon_s}, \tag{101}$$

where q is any of the four specific humidities q_{as}, q_{ai}, q_{ao}, and q_A. Furthermore, p_A is the local mean sea level pressure (in hPa) and ε_s is any of the saturated vapor pressures ε_s^{as} (at the atmosphere-snow interface), ε_s^{ai} (at the atmosphere-ice interface), ε_s^{ao} (at the atmosphere-ocean interface), and ε_s^A (in the atmosphere at 2m height) measured in in hPa. The latter three quantities are in turn parameterized in accord with *Gill* (1982, p. 606). Let

$$f_w(T) = 1 + 10^{-8} p_A (4.5 + 0.0006T^2), \tag{102}$$

and

$$\beta_1(T) = \frac{0.7859 + 0.03477T}{1 + 0.00412T}, \quad \beta_2(T) = 0.00422T \tag{103}$$

be functions of the temperature T (in ^oC), then

$$\varepsilon_s^A = 10^2 f_w(T_{dew}) \begin{cases} 10^{[\beta_1(T_{dew})+\beta_2(T_{dew})]} & ; \; T_A < 0^oC \\ 10^{[\beta_1(T_{dew})]} & ; \; T_A \geq 0^oC \end{cases}, \tag{104}$$

$$\varepsilon_s^{ao} = 0.98 \cdot 10^2 f_w(T_{ao}) \cdot 10^{\beta_1(T_{ao})}, \tag{105}$$

and

$$\varepsilon_s^{as,ai} = 10^2 f_w(T_{as,ai}) \cdot 10^{[\beta_1(T_{as,ai})+\beta_2(T_{as,ai})]}, \tag{106}$$

where T_{dew} is the dew point temperature input from the atmospheric forcing). Note that in (104), (105), and (106) the temperatures T_{dew}, T_{as}, T_{ai} and T_{ao} are all in ^oC on input.

9.3.5 Sensible heat fluxes $Q_{Se}^{as,ai}$ and Q_{Se}^{ao}

The sensible heat fluxes are somewhat simpler and are parameterized according to

$$Q_{Se}^{as,ai} = \rho_A c_{pa} C_S^a |\mathbf{U}_a| (T_{as,ai} - T_A) \; , \; Q_{Se}^{ao} = \rho_{Af} c_{pa} C_{Sf}^{ao} |\mathbf{U}_a| (T_{ao} - T_A). \tag{107}$$

Here ρ_A is an atmospheric reference density (Table 8), ρ_{Af} is the air density as given by (41), c_{pa} the specific heat capacity of the atmosphere (Table 11), while C_{Sf}^{ao} and C_S^a are transfer coefficients of sensible heat over open water and ice/snow, respectively. While C_S^a is given in Table 11, C_S^{ao} is related to the similar coefficient C_{Lf}^{ao} for latent heat flux through the relation

$$C_{Sf}^{ao} = 0.95 \cdot C_{Lf}^{ao}. \tag{108}$$

where C_{Lf}^{ao} is given in (97).

10 Salinity fluxes

When sea-ice freezes, when snow and/or ice melts and when there is precipitation whether in the form of rain (wet precipitation) or snow (frozen precipitation), it affects the salinity in the upper ocean mixed layer. In MI-IM these processes are translated into salinity fluxes that all contributes to a combined or net salinity flux that is exchanged with the ocean model. In accord

with the heat flux notation the salinity flux in the portion of a unit area covered by ice is denoted F_O^{io} (that is, the flux from the ocean toward the ice-ocean interface), while the salinity flux in the portion of a unit area covered by open water is denoted F_O^{ao}. Hence the total or net salinity flux per unit area, denoted F_O, is[8]

$$F_O = AF_O^{io} + (1 - A)F_O^{ao} \tag{109}$$

The above mentioned processes are all computed as production rates as detailed in Section 7. At the ice-ocean interface ice is produced at a rate W_{io} which is positive under freezing and negative under melting. At the atmosphere-ocean interface ice can only be formed (freezing) which occurs at the rate W_{ao}. At the atmosphere-ice/snow interface ice and/or snow can melt only (negative production). This is given by the rate W_{as} for snow and W_{ai} for ice. Like W_{ao} both W_{as} and W_{ai} are defined as positive definite quantities.

10.1 Ice-ocean interface

As mentioned above (e.g., Section 5.4.1) some of the salt in the sea water is captured in small pockets forming a salty solution referred to as brine pockets when ice is formed. The sea-ice is therefore saline, but with a salinity s_I substantially less than sea water (Section 5.4). When ice melts at the ice-ocean interface the salt in the brine pockets are deposited into the upper ocean mixed layer. While the former process (freezing) extracts salt and hence increases the salinity in the upper ocean mixed layer, the latter process (melting) in effect expels low salinity water to the upper ocean mixed layer and hence decreases its salinity. Similarly, if ice melts at the atmosphere-ice interface, snow melts at the atmosphere-snow interface and/or is dumped into the ocean due to lateral ice melt (snow run off), and, as in MI-IM, is transferred directly into the upper ocean mixed layer, it decreases the salinity of the upper ocean mixed layer. The latter is also true when wet precipitation (rain) falls on the ice covered portion of a unit area (freshwater source). Snow fall on the other hand is used to increase the snow thickness, which may later melt. In summary the contribution to the net salinity flux from the ocean toward that portion of a unit area covered by ice is

$$F_O^{io} = F_O^{io,mf} + F_O^{io,sm} + F_O^{io,r}, \tag{110}$$

where $F_O^{io,mf}$ is the flux due to melting and freezing of ice at the ice-ocean interface, $F_O^{io,sm}$ is the flux due to ice/snow melt and/or snow run off, and $F_O^{io,r}$ is the flux due to precipitation.

To translate these processes in terms of salinity flux contributions consider first the process of ice freezing at the ice-ocean interface. This occurs at a rate $W_{io} > 0$, and hence the volume that freezes in a time step Δt is therefore $W_{io}\Delta t$. Let the salinity of the upper ocean mixed layer at time t be s_O^n and at time step $t + \Delta t$ after ice formation be $s_O^{n+1} = s_O^n + \Delta s_O$. Then

$$s_O^{n+1}(h_O^n - W_{io}\Delta t) = s_O^n h_O^n - s_I W_{io}\Delta t, \tag{111}$$

where h_O^n is the upper ocean mixed layer thickness at time t. Thus this process contributes to a time rate of change in the upper ocean mixed layer salinity given by

$$\partial_t s_O = \frac{W_{io}}{h_O^n}(s_O^n - s_I). \tag{112}$$

[8] In the FORTRAN code F_O is denoted FS (fs)

Thus, as expected, the salinity in the upper ocean mixed layer increases when freezing takes place ($W_{io} > 0$). Thus the resulting salinity flux must be *negative* (directed downward and away from the ice-ocean interface). Performing a similar derivation for melting conditions, in which case $W_{io} < 0$, yields exactly the same expression, and hence (112) is valid for both melting and freezing conditions. Hence the contribution to the net salinity flux due to melting and/or freezing of ice from below is

$$F_O^{io,mf} = -W_{io}(s_O - s_I). \tag{113}$$

Hence, it is positive (directed upward toward the ice-ocean interface) when ice is melting ($W_{io} < 0$) and negative (downward) when ice is freezing ($W_{io} > 0$). As required (110) therefore implies a decrease in the upper ocean mixed layer salinity under melting (positive flux) and an increase under ice formation (negative flux).

In the spring the snow accumulated throughout the winter starts to melt at a rate W_{as}. Later when all the snow has melted ice starts to melt from above at a rate W_{ai}. Furthermore when ice melts it also changes the ice concentration (lateral melting) in which case the surplus snow is dumped into the ocean rather than changing the snow thickness, and hence gives rise to a snow run off production rate denoted W_{ro} (Section 7.3). Following the procedure used in the preceding paragraph all of these processes may be translated into salinity fluxes in a fashion similar to (113). Hence their contribution to the salinity flux is

$$F_O^{io,sm} = (W_{as} + W_{ro})s_O + W_{ai}(s_O - s_I), \tag{114}$$

remembering that all the rates entering (114) are defined as positive definite quantities[9].

Finally, rain falling on the ice and/or snow, in contrast to snow fall, is not allowed to remain on the ice. Thus it is immediately transferred to the ocean as wet precipitation. It therefore yields a contribution to the salinity flux given by

$$F_O^{io,r} = W_r s_O, \tag{115}$$

which when added to the other two contributions (113) and (114) thus gives a net salinity flux from the ocean toward the ice-ocean interface by

$$F_O^{io} = (W_{ai} - W_{io})(s_O - s_I) + (W_{as} + W_{ro} + W_r)s_O. \tag{116}$$

10.2 Atmosphere-ocean interface

At the atmosphere-ocean interface the processes that contributes to a change in the upper ocean mixed layer is freezing of ice at a rate W_{ao}, and both wet and frozen precipitation at the rates W_r and W_s, respectively. Again all of these rates are defined as positive definite quantities (Section 5.1). The contribution from these processes is translated to salinity fluxes exactly as outlined in the preceding section. Hence the net salinity flux from the ocean toward the atmosphere-ocean interface is

$$F_O^{ao} = -W_{ao}(s_O - s_I) + (W_r + P_{snow})s_O + W_{ro}s_O. \tag{117}$$

[9] In similarity with (110) the snow melt contribution may be written $(W_{ro} + W_{as})(s_O - s_f)$ where $s_f = 0$ is the salinity of freshwater.

The first contribution on the right-hand side of (117) is always directed downward (negative) and therefore, as expected, gives rise to an increase in the upper ocean mixed layer salinity whenever ice is formed on the atmosphere-ocean interface. The remaining contributions are all freshwater sources, and hence they give rise to a decrease in the upper ocean mixed layer salinity.

Using (109) the net salinity flux per unit area transferred to the ocean model is

$$F_O = \left[A(W_{ai} - W_{io}) - (1-A)W_{ao}\right](s_O - s_I) + \left[W_{ro} + W_r + AW_{as} + (1-A)P_{snow}\right] s_O. \tag{118}$$

11 Verification

As outlined in Section 1 the above integrated flux and sea-ice model is intended as the ice-ocean component of a coupled atmosphere-ocean regional climate model (AORCM) system within the Norwegian national climate project RegClim. Thus, to verify that the developed ice-ocean component is stable under quasi-steady forcing a thirty year run is performed using a specified quasi-steady atmospheric input as forcing. To make the forcing quasi-steady the ECMWF operational analysis for the two years 2000 and 2001 is wrapped into thirty years and used as input. The wrapping is performed by supplying the two years in a repeated cycle starting January 1, 2000. The model response should therefore, after some initial adjustment, come to a quasi-equilibrium stage in which the sea-ice and at least the upper water mass circulation and hydrographic conditions repeat themselves on a two year cycle.

11.1 The model ocean

As alluded to the ocean model used is a version of the Miami Isopycnic Coordinate Ocean Model (MICOM), which is a dynamic-thermodynamic ocean general circulation model developed by *Bleck et al.* (1992, see also references therein). The model solves the primitive equations, using a split-explicit numerical scheme (*Bleck and Smith*, 1990), and is in the horizontal discretized on a C-grid. In the vertical MICOM uses potential density as the coordinate. The present implementation has 26 isopycnic layers in addition to the top mixed layer. The density of the interior isopycnic layers is determined based on densities from the area covered by the computational domain. It includes the very low salinity waters of the Baltic as well as the high salinity deep water of the Mediterranean. The upper mixed layer interacts with the atmosphere as well as the sea-ice as described in the preceding sections. It also interacts with the interior layers through entrainment/detrainment processes when the mixed layer deepens/retreats based on the bulk representation by *Gaspar et al.* (1990). The isopycnic interior layers interact mainly through hydrostatic pressure forces, but there is also a vertical flux due to a specified diapycnal mixing dependent on $1/N^2$ where N is the Brunt-Väisälä frequency (*McDougall and Dewar*, 1998). Thus the MICOM version using the vigorous Richardson dependent mixing scheme suggested by *Hallberg* (1999) and implemented in MICOM as described in *Shi and Røed* (2000) is not used here. This has some important consequences for the bottom water of the North Atlantic as shown below.

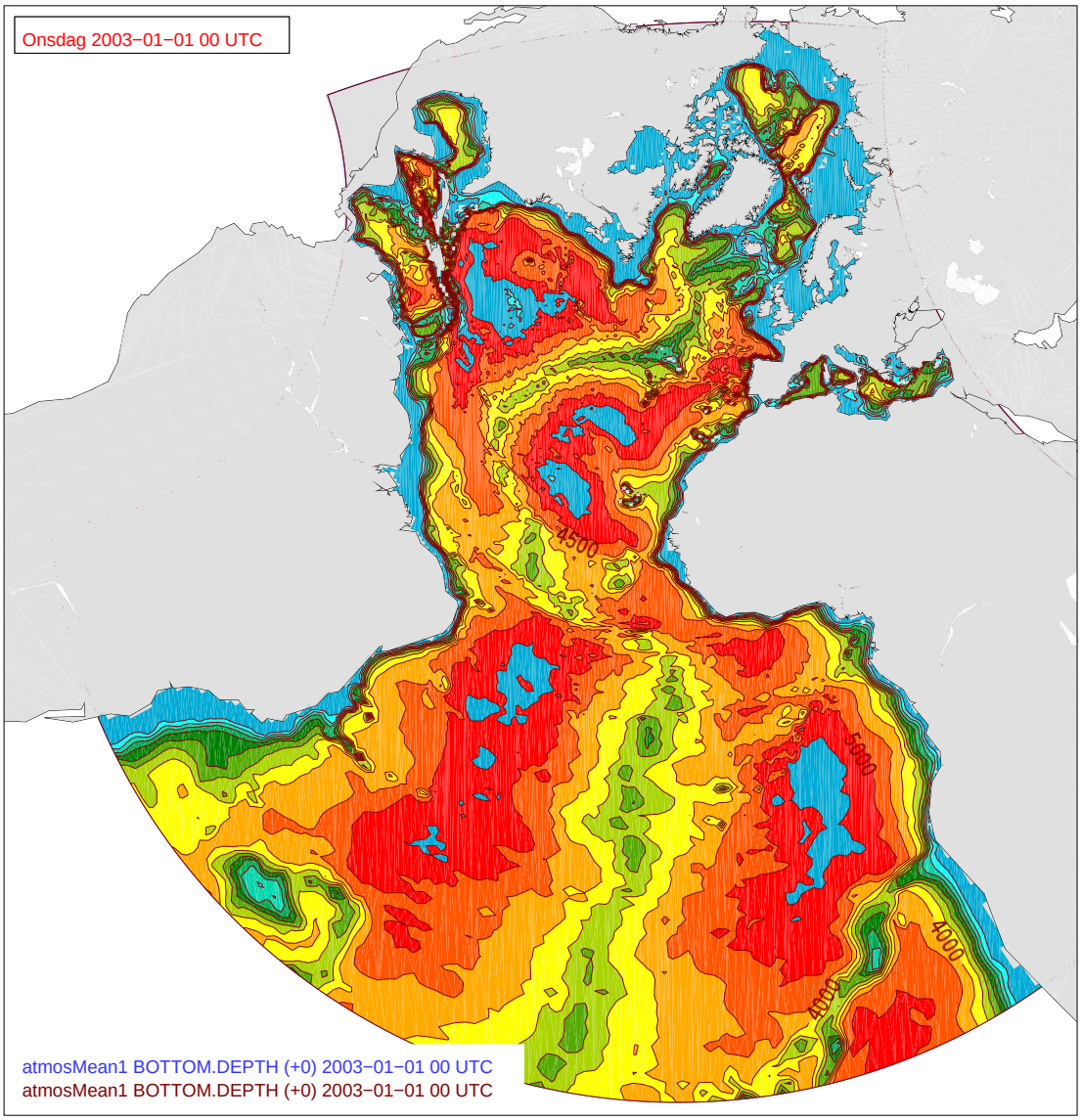

Fig. 3: Computational domain of the Atlantic MICOM used in the coupled regional atmosphere-ocean climate model (AORCM). Colors indicate depth with contour interval of 500 m. Only 10 colors are available so colors are wrapped. The blue color in the deep basins indicates depths greater than 5500 m, while the blue color close to land indicates depths less than 500 m.

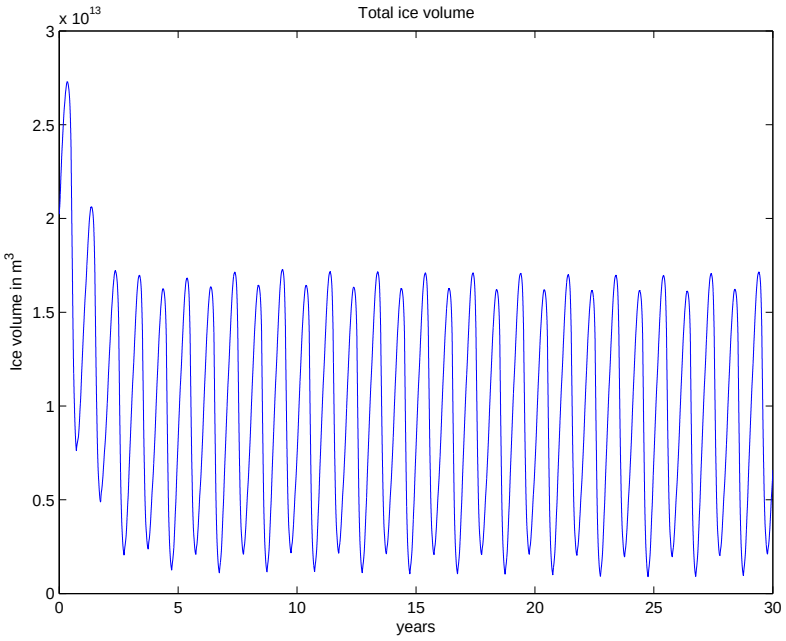

Fig. 4: Solid (blue) line shows the time evolution of the total ice volume for the thirty year verification run with the coupled ice-ocean model MI-IM. Note the apparent two year repeat cycle. This is due to the applied meteorological forcing which is the ECMWF operational analysis for the years 2000 and 2001. Also note that after about five years of integration the coupled model reach a quasi-equilibrium state.

The computational domain for the verifi cation run is shown in Figure 3. It covers the Arctic Ocean, the Nordic Seas, and the Atlantic Ocean north of about 30^oS. At the wide open boundary to the south temperature and salinity is specifi ed according to Levitus' climatology, and transferred to the model via a relaxation buffer zone. About 35 of the major rivers within the domain is supplied to the model by specifying its volume of water as "precipitation" of freshwater with a certain temperature (*Debernard and Røed*, 2002). The temperature of the river was determined using the Levitus climatological temperature at the grid point where the river was specifi ed to discharge, but limited downward to 0^oC. A similar procedure was used to mimic the influx through the Bering Strait in which water of salinity and temperature in accord with the Levitus climatology is specifi ed with a volume of about $1.1Sv$ ($1Sv = 10^6 m^3 s^{-1}$). This way both the river efflux into the model domain and the Bering strait inflow manifests as barotropic as well as baroclinic forcing. This is in contrast to, e.g. *Haugen et al.* (2002), where only the baroclinic forcing was provided.

The grid is a rotated spherical grid with mesh size $1/2^o$. The 'North Pole' is located in the Indian Ocean at 15^oN and 95^oW. Thus the resolution is relatively coarse (not even close to being eddy permitting in the area of interest) with the grid size being about 55 km in the 'meridional' direction and varying from slightly above 22 km to 55 km in the 'zonal' direction (Figure 3). While the ocean model was initialized from the Levitus climatology, the sea-ice was simply specifi ed to be a uniform slab of volume $Ah = 2$m and having a concentration of $A = 90\%$.

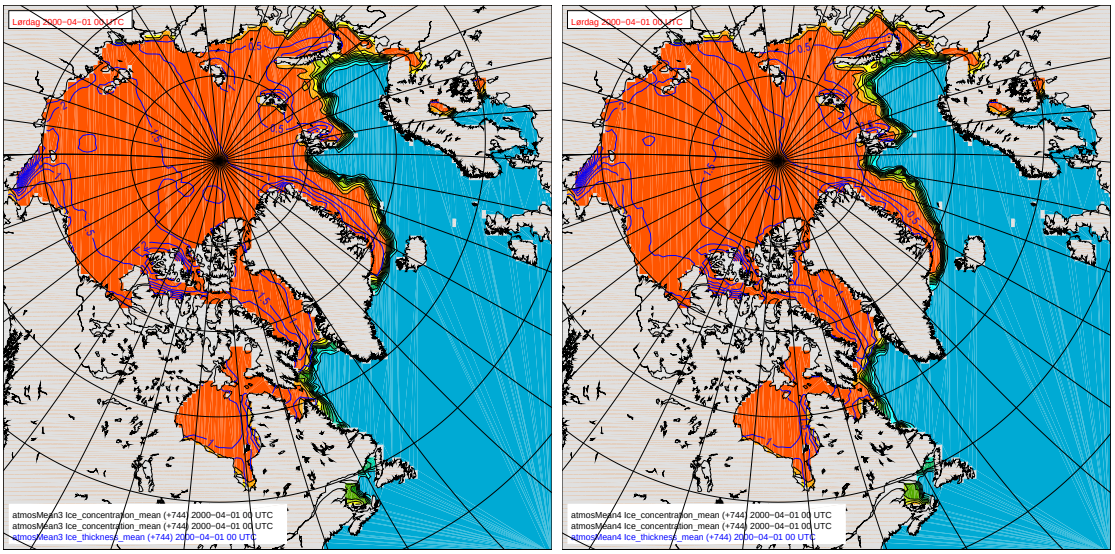

Fig. 5: Monthly mean sea-ice concentration (colors) and thickness (solid blue lines) for March of year 7 (upper panel) and year 27 (lower panel).

Also the sea ice is initially confi ned to areas where the sea surface temperature (SST) is less than -0.5^oC. Initially the ice is snow covered with a uniform thickness of $h_S = 10$cm.

11.2 Results

11.2.1 Sea-ice

The evolution of the total ice volume throughout the thirty years integration is displayed in Figure 4. After a period of about fi ve years of initial adjustment the total ice volume appears to repeat itself on a two year cycle, the fi rst year (2000) in the cycle being slightly different from the second year (2001).

That the ice volume repeats itself is also evident by looking at Figure 5, which shows the monthly mean ice concentration and thickness for the month of March for the years 7 and 27, that is, for two years twenty years apart. A similar composite is shown in Figure 6, but then for the month of September. It is fi rst noted that although there are differences in the details between the two years, they exhibit remarkably similar ice conditions, for instance in its extension, concentration and thickness. In March the ice extends over most of the Arctic Ocean with a concentration of about 90-100%, and with a thickness of about 1.5 to 2 meters in both years. The Davis Strait is kept ice free and so are the areas west of Spitsbergen as well as most of the Barents Sea. Furthermore, also the areas along the southeast coast of Greenland and the areas along the eastern coast of Canada in the Labrador Sea are ice free. It is also noted that the Baltic exhibits an ice cover in the Bothnia Bay and in the Finnish Bay only, and that the Hudson Bay is 90-100% ice covered with 1- 1.5 meter thick ice.

In September (Figure 6) the ice extent is considerably less, but still remarkably similar for

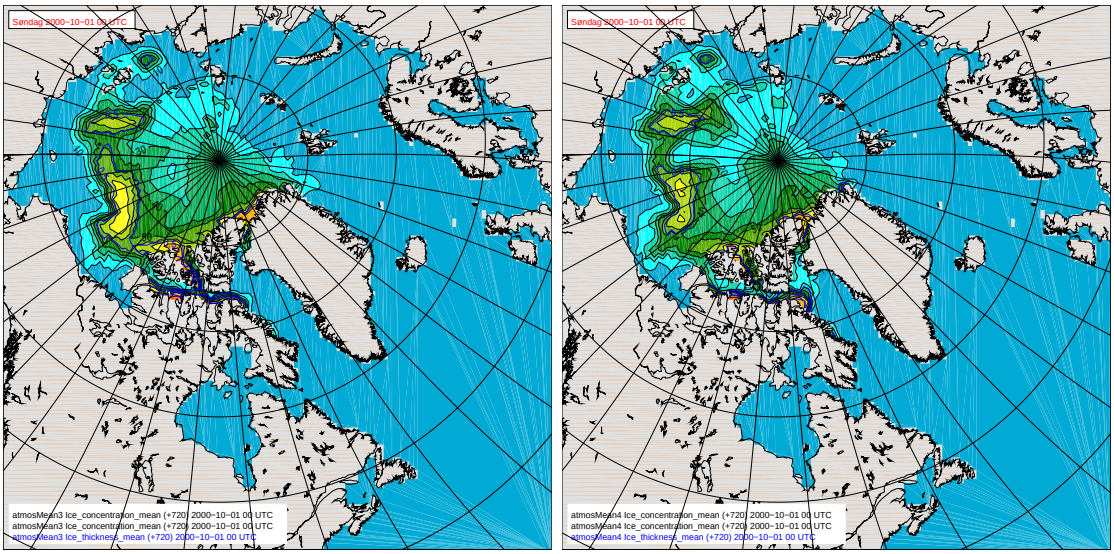

Fig. 6: Monthly mean sea-ice concentration (colors) and thickness (solid blue lines) for September of year 7 (left panel) and year 27 (right panel).

the two years in its gross features. The Baltic is now ice free, and so is the Hudson Bay and the Barents, Kara and Chukchi Seas as well as most of Baffi n Bay. In the Arctic Ocean the ice cover has retreated away from most of the coastal areas all around the Arctic except along the Canadian Archipelago. Only in this area and in parts of the Beaufort and Laptev Seas is the ice concentrations above 20%, the ice concentration at the North Pole itself being between 30 and 40%. Finally, it is noted that the thickness in September is less than one meter even in those areas where the concentrations are above 70%.

These concentrations may also be compared with observations. To this effect the observed average monthly mean ice concentration for the ten years 1978-87 (*Gloersen et al.*, 1992) based on satellite imagery may be used. As revealed by comparing Figure 5 with that of the month of March from *Gloersen et al.* (1992, Fig. 3.1.15, p. 70), it is evident that the gross features are similar. For instance the ice in the Baltic and in the Finnish Bay is in place, and the waters west of Spitsbergen are ice free. There are also important discrepancies. For instance the ice does not extend far enough south along East Greenland and along the eastern coast of Canada in the Labrador Sea. This could be related to fact that the model Gulf stream (Section 11.2.2) is situated further north than observed, and hence warm water is advected too far north in these two areas.

A similar comparison for the month of September, comparing Figure 6 with that of *Gloersen et al.* (1992, Fig. 3.1.15, p. 70), reveals that although the gross features are in place, the ice extent is too small, in that the ice edge is located much further north than observed. It should be noted that the sea ice melt during summer very sensitive to the amount of shortwave radiation input. This in turn depends on the cloud parameterization, the surface albedo parameterization, the amount of frozen precipitation that falls during winter, etc. Thus, although a detailed calibration of the various parameterizations is needed, also a detailed analysis of the actual atmospheric

input, here the ECMWF operational analysis, in terms of amount of frozen precipitation and cloud fraction is called for.

Finally it should be mentioned that although observations of ice thickness is not that well documented, the ice thicknesses both in winter and summer as revealed by Figures 5 and 6 appear to be way too small, in particular in the area close to the Canadian Archipelago. This may partly be due to the initial condition, in which the ice is specifi ed as a slab of volume 2 meter and concentration 90%. Exploratory experiments indicates that also the neglect of frazil ice formation may be of importance to rectify the response in this respect. Also varying the empirical constant in (7) is an option. These are to some degree tuning factors which are model as well as model application dependent. For instance by decreasing the second of these, Φ_2, the production of open water is increased which in turn implies that more ice is produced.

11.2.2 Sea surface temperature and currents

The models response in terms of the monthly mean sea surface temperature (SST) and currents for February of year 27 is displayed in Figure 7. As is evident the model Gulf Stream appears to be located north of its expected path along the northeastern coast of North America, resulting in warm water being advected too far north. This probably explains why the model tends to give too little ice along the eastern coast of Canada in the Labrador Sea and along the southeastern part of the Greenland coast. However, comparing the monthly mean SST for the same month twenty years apart as revealed by Figure 7 it is satisfying to note that the two SST patterns are very similar indeed. This again underscores the fact that after the initial adjustment the upper water mass conditions repeats themselves on a two year cycle.

Figure 7 also reveals the well known pattern of colder water upwelling along the equator. This is necessary to obtain the well known equatorial current structures with a well developed equatorial counter-current north of equator.

11.2.3 Bottom layers

Initially the bottom waters of the Norwegian Sea, which in the present set-up corresponds to layer 25 water masses, is not present in the North Atlantic deep water. However, as revealed by Figure 8 (left panel) this layer is already present there after three years of integration as three elongated fi ngers. These fi ngers clearly extend from the Denmark Strait, the Faeroe-Bank Channel and the Wyville-Thomson ridge (just west of Scotland), and are evidence of the overfbw of Norwegian Sea Deep Water (NSDW). After about 15 years of integration (Figure 8, right panel) the overfbw is quite extensive and is present in particular in the eastern basin of the North Atlantic. The presence of these very dense water masses in the North Atlantic is an artifact. As noted by *Hallberg* (1999) and *Shi et al.* (2001) the canonical MICOM version used here does not have a parameterization of diapycnal mixing which is able to properly account for the vigorous and turbulent mixing that takes place close to the bottom when the NSDW overfbws the Greenland-Scotland ridges. As an implication the dense bottom layer containing the NSDW does not collapse downstream of the sills, but shows up as a fi nite depth layer in the North Atlantic. Rather than implementing the somewhat computationally expensive scheme of *Shi et al.* (2001)

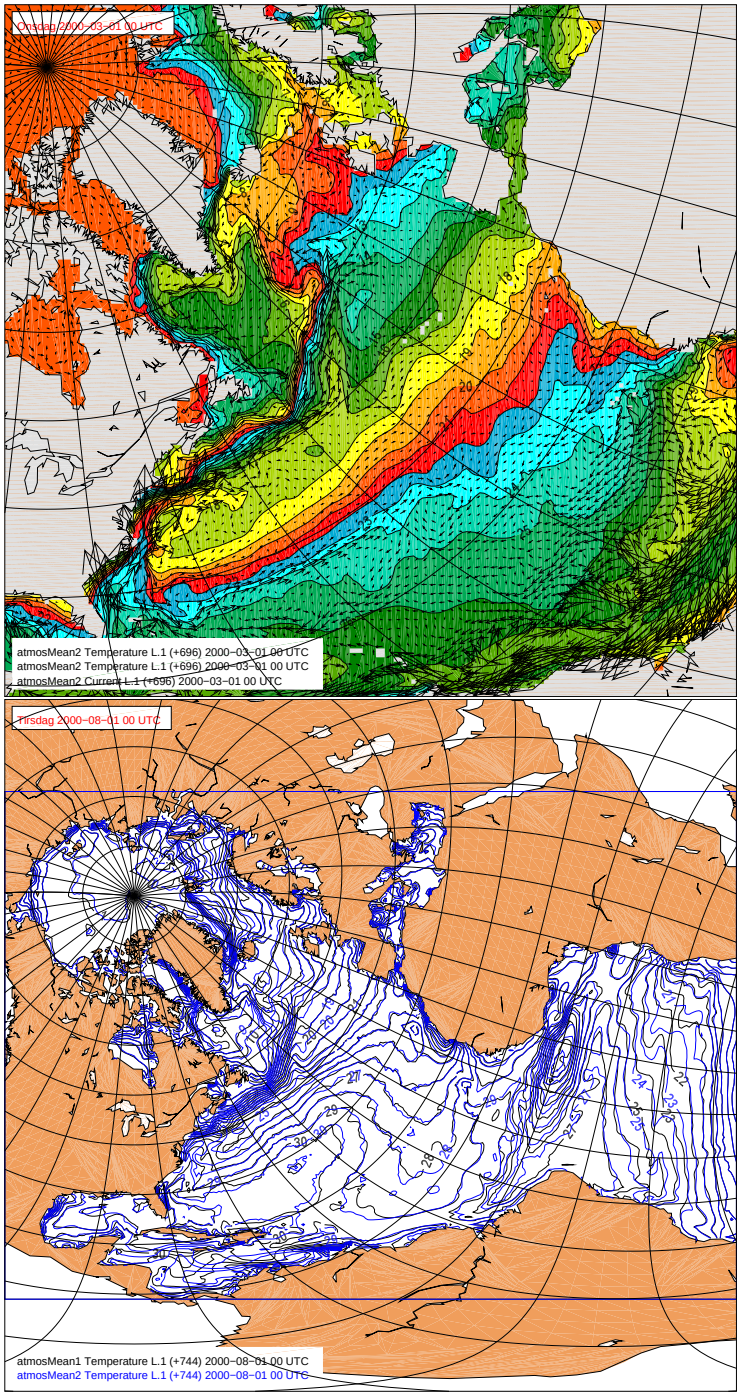

Fig. 7: Panel a shows monthly mean SST (colors with interval of 1 ^{o}C) and currents (black arrows) for February of year 27. Note that coloring is wrap around, so that the ten colors present repeats themselves when the SST difference becomes larger than 10^{o}C (as it does). Panel b shows a comparison of the SST for the month of July for two years twenty years apart.

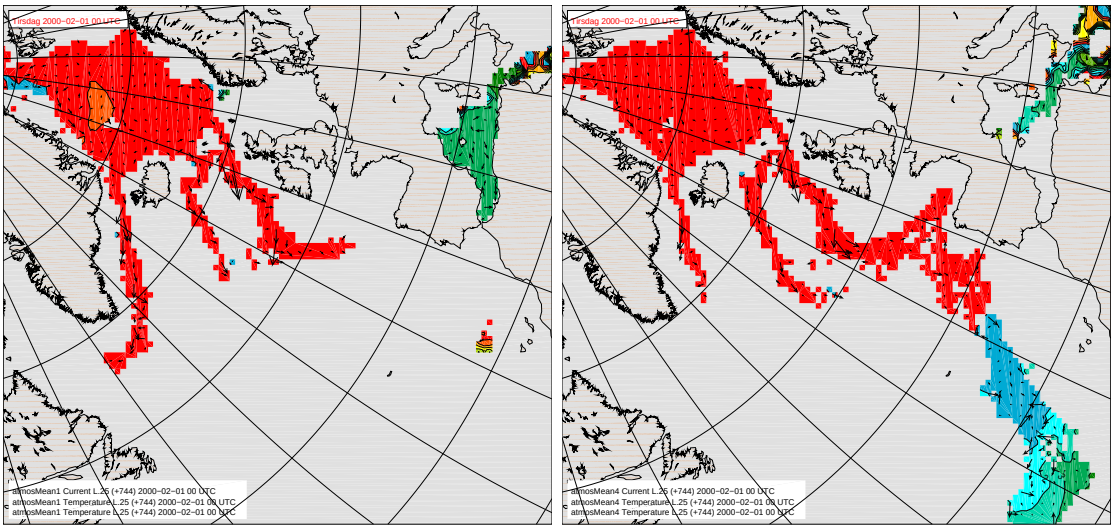

Fig. 8: Temperature (colors) and currents (black arrows) in MICOM's layer number 25 after three years (left panel) and 15 years of integration (right panel). It also conveniently shows the distribution of this layer. Note that the water masses of layer number 25 corresponds to the deep water in the Norwegian and Mediterranean Seas and was initially present only in these basins. Since the Mediterranean deep water is warmer than the NSDWNote that although both layers have the same density the Mediterranean Sea water is much warmer and is only present as one bolus west of Africa.

the diapycnal mixing rate in the bottom layers may simply be increased. This could cause layer 25, which is at the bottom of the Norwegian Sea to collapse downstream of the sills.

Also the even denser Mediterranean deep water has overflowed across the sill in the Strait of Gibraltar (not shown). Evidence of this is found by looking at the temperature distribution in layer 25 after 15 years of integration (Figure 8, right panel). The southern part of the finger has clearly received warmer and saltier water from beneath (and also warmer fresher water from above due to the dual entrainment scheme) as it overlays the Mediterranean deep water that has overflowed into the abyssal plain off the West Africa (the Cape Verde and Madeira abyssal plains).

11.2.4 Discussion

It should be kept in mind that the present experiment is a verification experiment and not a validation exercise. Thus, although some of the results shown above are not satisfactorily as a validation, they clearly shows that the coupled system and the integrated flux module is working and giving reasonable results. Particularly important in this respect is that the model system, when forced with a repeated two year meteorological input, reaches a quasi-equilibrium state in which the model response also exhibits a two year repeat cycle. The exception from this picture is the overflow of Norwegian Sea Deep Water across the Greenland-Scotland Ridges that spreads in the North Atlantic, in particular in the eastern North Atlantic. This is an inherent artifact of the MICOM model when used in its canonical form and serves here to verify that the model system

actually behaves as expected.

To conclude the results are satisfying and verifies that the model system and its integrated air-sea flux module is working properly. It should be noted, however, that some further calibration and tuning of the system is still needed to make the results fall more in line with observational evidence. In particular this pertains to the excessive melting of ice in the summer and to the amount if ice production in winter. Other less satisfying result when compared to observational evidence is the location of the Gulf Stream, and the excessive overflow of NSDW. As revealed by for instance by *Hurlburt and Hogan* (2000) and others the former is an artifact of the resolution. Our resolution is about 60 km in the Gulf stream area, clearly too large compared to 4 km resolution they suggest to be appropriate.

12 Final remarks

Documented above is a recently developed dynamic-thermodynamic sea-ice model integrated with a flux module calculating the necessary air-sea fluxes. The model is named the Norwegian Meteorological Institutes Ice Model (MI-IM). While the sea-ice dynamics are based on on the ideas of *Hunke and Dukowicz* (1997), the thermodynamics are based on the ideas of *Häkkinen and Mellor* (1992). The parameterization of the incoming shortwave solar radiation is similar to that described in *Drange and Simonsen* (1996). The remaining fluxes are bulk formulas based on the recent work of *Kara et al.* (2000). This documentation pertains to the version of MI-IM coupled to the ocean model MICOM (*Bleck et al.*, 1992). A slightly modified version has also been coupled to the ocean model MI-POM (Norwegian Meteorological Institutes version of the Princeton Ocean Model) with success.

The developed coupled ice-ocean model is verified by performing a thirty year integration. The meteorological input used is the ECMWF operational analysis for the two years 2000 and 2001 which are repeatedly applied to cover the thirty year period. Results from this experiment shown in Section 11 demonstrate that the developed model system is working in accord with its design. In particular it is worthwhile mentioning that the response of the coupled model establish a quasi-equilibrium state after about five years of integration that repeats itself on a two year cycle, at least when it comes to conditions related to the ice and the upper water masses.

The model response is also compared with satellite observations of ice concentration, and against common knowledge about the general Atlantic Ocean circulation and hydrography, e.g., the Gulf Stream, with mixed results. However, here the focus is on verification rather than validation, and hence the fact that the model response repeats itself on a two year cycle and does not give any trend is satisfying. Also that the gross features are correct and that discrepancies may be explained in failure to represent the location of the Gulf stream correctly is satisfying.

Acknowledgment: This work is funded in part by the Research Council of Norway (RCN) and in part by the EU 5th Framework programme (FP5). The RCN funding is through the the national climate project RegClim (Regional development under global climate change, grant no. 120656/720; JD, LPR, JA, ØS) under the KlimaProg program, and the project MONCOZE

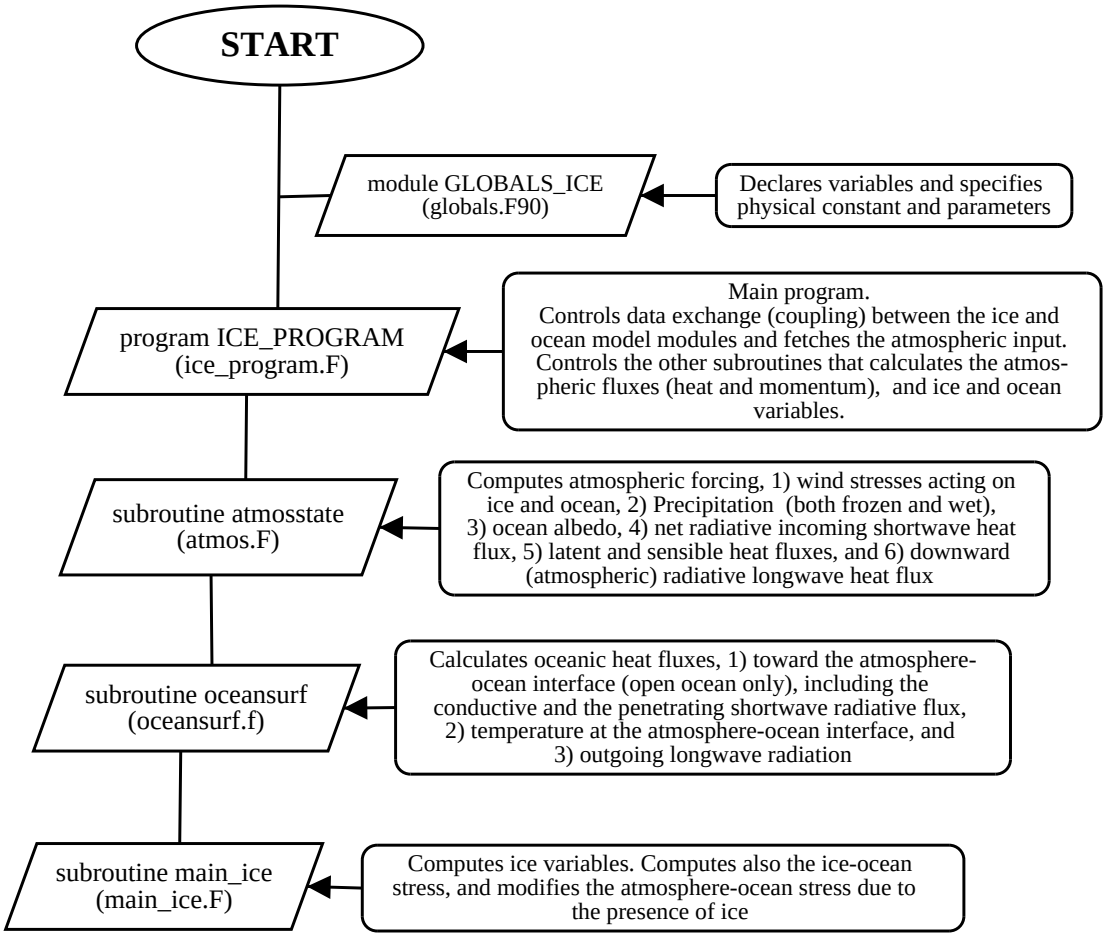

Fig. 9: Flowchart showing the program structure of MI-IM's main program. The name in parenthesis gives the concomitant FORTRAN program.

(Monitoring the Norwegian coastal zone environment, grant no.143559/431; JA and LPR). The FP5 funding is associated with the project GLIMPSE (Global implications of Arctic climate processes and feedbacks, grant no. EVK2-2001-00337; LPR, MØK).

APPENDIX

A Flowcharts

The structure of the FORTRAN code for MI-IM is shown in Figures 9, 10, and 11. Also included is a description of the purpose of each of the programs, subprograms and subroutines presented. Note that the fbwcharts are not complete. Most of the subprograms and subroutines in turn call other subroutines and functions not shown in the presented fbwcharts.

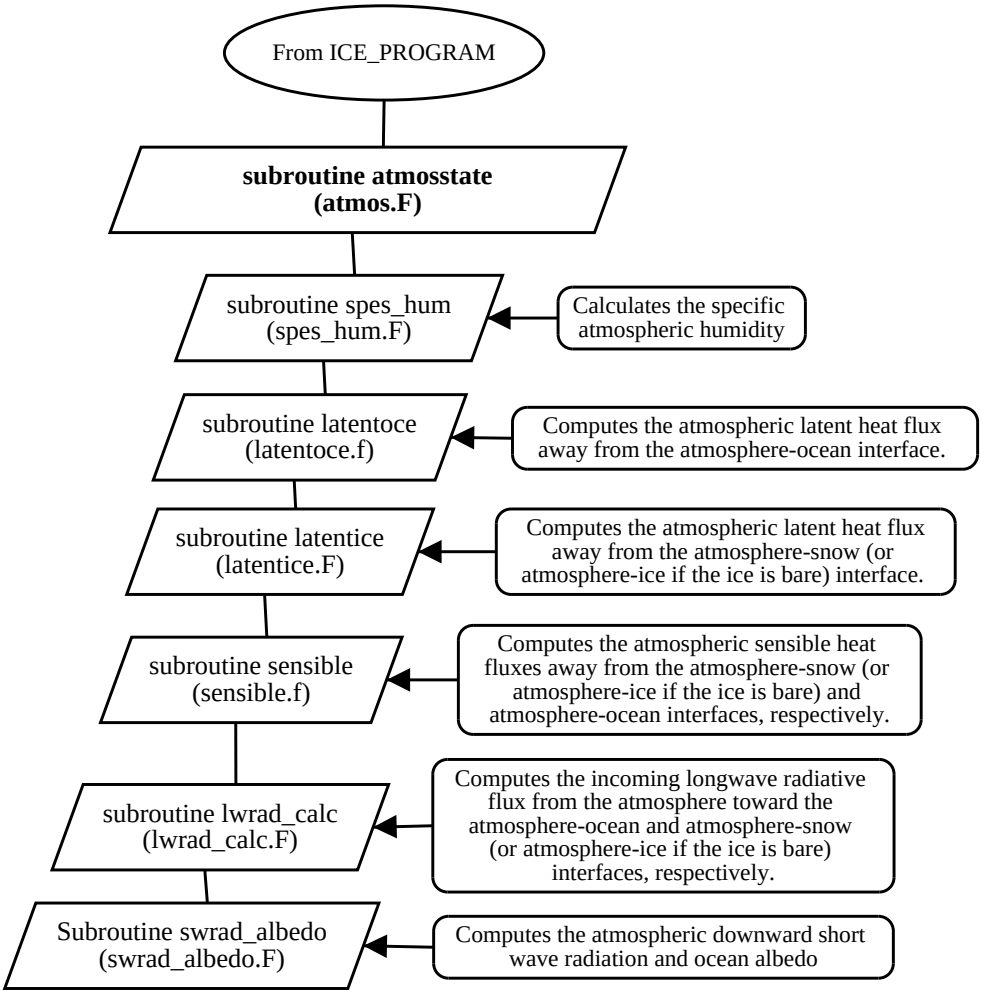

Fig. 10: Flowchart showing the program structure associated with the subroutine atmosstate. The name in parentheses gives the concomitant FORTRAN program.

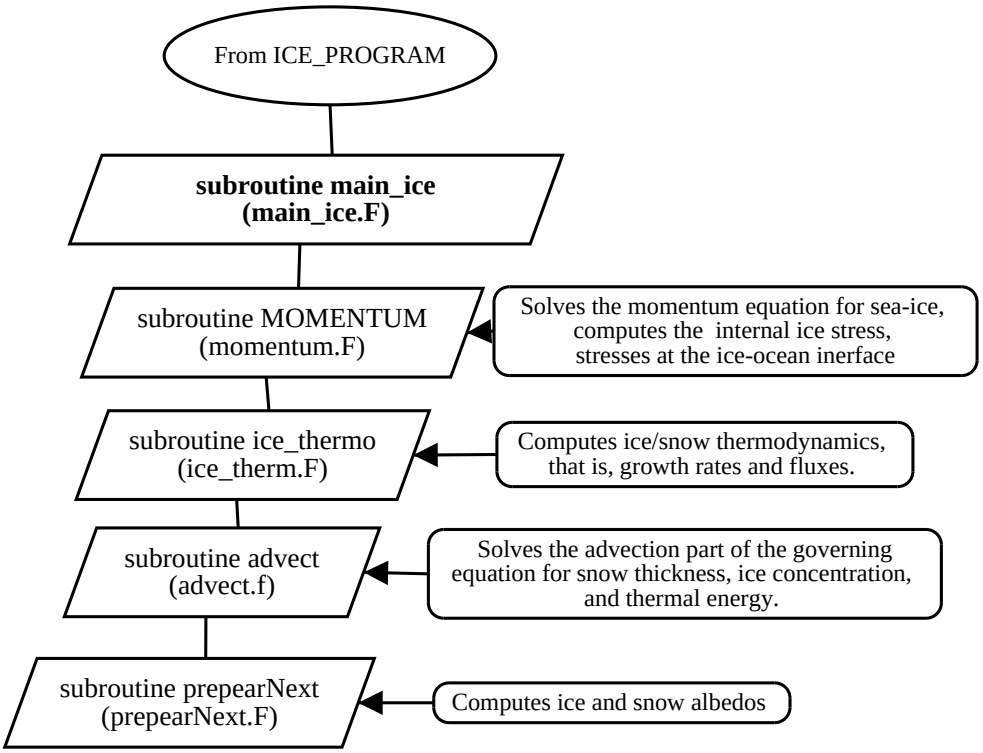

Fig. 11: Flowchart showing the program structure associated with the subroutine main_ice. The name in parentheses gives the concomitant FORTRAN program.

References

Bitz, C. M., and W. H. Lipscomb, An energy-conserving thermodynamic model of sea ice, *J. Geophys. Res.*, *104*, 15,669–15,677, 1999.

Bjørge, D., and V. Ødegaard, Empirical orthogonal functions analysis applied to MSLP from regional simulations, *Research Report 134*, Norwegian Meteorological Institute, 2000, ISSN 0332-9879.

Bjørge, D., J. E. Haugen, and T. E. Nordeng, Future climate in Norway, *Research Report 103*, Norwegian Meteorological Institute, 2000, ISSN 0332-9879.

Bleck, R., and L. Smith, A wind-driven isopycnic coordinate model of the north and equatioral Atlantic Ocean. 1. Model development and supporting experiments., *J. Geophys. Res.*, *95C*, 3273–3285, 1990.

Bleck, R., C. Rooth, D. Hu, and L. T. Smith, Salinity-driven thermohaline transients in a wind- and thermohaline-forced isopycnic coordinate model of the North Atlantic, *J. Phys. Oceanogr.*, *22*, 1486–1515, 1992.

Blumberg, A., and G. Mellor, A description of a three-dimensional coastal ocean circulation model., in *Three-dimensional Coastal Ocean Models*, edited by N. Heaps., vol. 4 of *Coastal and Estuarine Sciences*, American Geophys. Union, 1987.

Curry, J. A., W. B. Rossow, D. Randall, and J. L. Schramm, Overview of Arctic cloud and radiation characteristics, *J. Climate*, *9*, 1731–1764, 1996.

Debernard, J., and L. P. Røed, Implementation of rivers in met.no's MICOM-version by surface fluxes, *Tech. Rep. 6*, RegClim General Technical Report, 2002, [Available from Norwegian Institute for Air Research, POBox 100, N-2027 Kjeller, Norway].

Debernard, J., Ø. Sætra, and L. P. Røed, Future wind, wave and storm surge climate in the northern North Atlantic, *Climate Res.*, *23*, 39–49, 2002.

Denis, B., R. Laprise, D. Caya, and J. Coté, Downscaling ability of one-way nested regional climate models: the big brother experiments, *Climate Dyn.*, *18*, 627–646, 2002.

Drange, H., and K. Simonsen, Formulation of air-sea fluxes in the ESOP2 version of MICOM, *Tech. Rep. 125*, NERSC, 1996, [Available from Nansen Environmental and Remote Sensing Center, Edv. Griegsvei 3A, N-5037 Bergen, Norway].

Ebert, E. E., and J. A. Curry, An intermediate one-dimensional thermodynamic sea ice model for investigating ice-atmosphere interactions, *J. Geophys. Res.*, *98*, 10,085–10,109, 1993.

Engedahl, H., Implementation of the Princeton ocean model (POM/ECOM-3D) at the Norwegian Meteorological Institute (DNMI)., *Research Report 5*, Norwegian Meteorological Institute, 1995.

Engedahl, H., A. Lunde, A. Melsom, and X. B. Shi, New schemes for vertical mixing in MI-POM and MICOM, *Research Report 118*, Norwegian Meteorological Institute, 2001, ISSN 0332-9879.

Fairall, C. W., E. F. Bradley, J. S. Godfrey, G. A. Wick, J. B. Edson, and G. S. Young, Cool-skin and warm-layer effects on sea surface temperature, *J. Geophys. Res.*, *101*, 1295–1308, 1996.

Gaspar, P., Y. Gregories, and J.-M. Lefevre, A simple eddy kinetic energy model for simulations of the oceanic vertical mixing: Tests at station papa and long-term upper ocean study site, *J. Geophys. Res.*, *95*, 16,179–16,193, 1990.

Gill, A. E., *Atmosphere-ocean dynamics*, vol. 30 of *International Geophysical Ser.*, Academic Press, 1982.

Giorgi, F., B. Hewitson, J. Christensen, M. Hulme, H. von Storch, P. Whetton, R. Jones, L. Mearns, and C. Fu, Regional climate information - evaluations and projections, in *Climate Change 2001: The Scientific Basis*, edited by J. T. Houghton and et al., Cambridge University Press, 2001.

Gloersen, P., W. J. Campbell, D. J. Cavalieri, C. L. P. J. C. Comiso, and H. J. Zwally, *Arctic and Antarctic sea ice, 1978-1987*, vol. NASA SP No. 511 of *Scientific and Technical Information Program*, National Aeronautic and Space Administration, Washington D.C., 1992.

Grenfell, T. C., S. G. Warren, and P. C. Mullen, Reflection of solar radiation by the antarctic snow surface at ultraviolet, visible, and near-infrared wavelengths, *J. Geophys. Res.*, *99*, 18,669–18,684, 1994.

Häkkinen, S., and G. Mellor, Modeling the seasonal variability of a coupled Arctic ice-ocean system, *J. Geophys. Res.*, *97*, 20,285–20,304, 1992.

Hallberg, R., Time integration of diapycnal diffusion and Richardson number dependent mixing in isopycnal coordinate ocean models, *Mon. Weath. Rev.*, *00*, 00–00, 1999.

Haugen, V. E., O. M. Johannessen, and G. Evensen, Indian Ocean: Validation of the Miami Isopycnic Coordinate Ocean Model and ENSO events during 1958-1998, *J. Geophys. Res.*, *107*, 10,1029–10,1057, 2002.

Hibler, W. I., A dynamic-thermodynamic sea ice model, *J. Phys. Oceanogr.*, *9*, 815–846, 1979.

Hunke, E., and J. Dukowicz, An elastic-viscous-plastic model for sea ice dynamics, *J. Phys. Oceanogr.*, *27*, 1849–1867, 1997.

Hurlburt, H. E., and P. J. Hogan, Impact of $1/8^o$ to $1/64^o$ resolution on Gulf Stream model-data comparisons in basin-scale subtropical Atlantic Ocean models, *Dyn. Atmos. Oceans*, *32*, 283–329, 2000.

Kara, B. A., P. A. Rochford, and H. E. Hurlburt, Effi cient and accurate bulk parameterizations of air-sea fluxes for use in general circulation models, *J. Atmos. Ocean. Tech.*, *17*, 1421–1438, 2000.

Kara, B. A., P. A. Rochford, and H. E. Hurlburt, Air-sea flux estimates and the 1997-1998 ENSO event, *Boundary -Layer Meteor.*, *103*, 439–458, 2002.

McAveney, B. J., C. Covey, S. Joussaume, V. Kattsov, A. Kitoh, W. Ogana, A. J. Pitman, A. J. Weaver, R. A. Wood, and Z.-C. Zhao, Model evaluation, in *Climate Change 2001: The Scientific Basis*, edited by J. T. Houghton and et al., Cambridge University Press, 2001.

McDougall, T. J., and W. K. Dewar, Vertical mixing cabbeling, and thermobaricity in layered models, *J. Phys. Oceanogr.*, *28*, 1458–1480, 1998.

Mellor, G., and L. Kantha, An ice-ocean coupled model, *J. Geophys. Res.*, *94*, 10,937–10,954, 1989.

Omstedt, A., and J. S. Wettlaufer, Ice growth and oceanic heat-flux: Models and measurements, *J. Geophys. Res.*, *97*, 9383–9390, 1992.

Overland, J., S. L. McNutt, S. Salo, J. Groves, and S. Lie, Arctic sea ice as a granular plastic, *J. Geophys. Res.*, *103*, 21,845–21,867, 1998.

Perovich, D. K., and T. C. Grenfell, Laboratory studies of the optical properties of young sea ice, *J. Glaciology*, *27*, 331–346, 1981.

Røed, L., H. Engedahl, B. Hackett, A. Melsom, X. Shi, and Ø. Sætra, Circulation and hydrography in the Nordic Seas inferred from ocean model experiments at DNMI, *Tech. Rep. 2*, RegClim General Technical Report Series, 1999, [Available from Norwegian Institute of Air Research, P.O. Box 100, N-2007 Kjeller, Norway].

Røed, L. . P., and I. Fossum, Mean and eddy motion in the Skagerrak/northern North Sea: insight from a numerical model, *Ocean Dynamics*, *in press*, 2003.

Rogers, R. R., and M. Yau, *A short course in cloud physics - 3rd*, vol. 113 of *International series in natural philosophy*, Pergamon Press, 1989.

Rosati, A., and K. Miyakoda, A general-circulation model for upper-ocean simulations, *J. Phys. Oceanogr.*, *18*, 1601–1626, 1988.

Sætra, Ø., C. Wettre, and L. Røed, Coupled ice-ocean modelling, *Tech. Rep. 1*, RegClim General Technical Report Series, 1998, [Available from Norwegian Institute of Air Research, P.O. Box 100, N-2007 Kjeller, Norway].

Sætra, Ø., L. Røed, and J. Albretsen, The DNMI RegClim ice model, *Tech. Rep. 3*, RegClim General Technical Report, 1999.

Shi, X. B., and L. P. Røed, Documentation of DNMI's MICOM version, part 3: Implementation of a Richardson number dependent mixing scheme, *Tech. Rep. 95*, Norwegian Meteorological Institute, 2000, [Avaialable from Norwegian Meteorological Institute, Postboks 43 Blindern, N-0313 Oslo, Norway].

Shi, X. B., L. P. Røed, and B. Hackett, Variability of the Denmark Strait overflow: a numerical study, *J. Geophys. Res.*, *106*, 22,277–22,294, 2001.

Smolarkiewicz, P., and L. Margolin, MPDATA: a finite difference solver for geophysical flows, *J. Comp. Phys.*, *140*, 459–480, 1997.

Smolarkiewicz, P. K., A simple positive definite advection scheme with small implicit diffusion, *Mon. Wea. Rev.*, *111*, pp. 479, 1983.

Tschudi, M., J. Curry, and J. Maslanik, Airborne observations of summertime surface features and their effect on surface albedo during FIRE/SHEBA, *J. Geophys. Res.*, *106*, 15,335–15,344, 2001.